EFFECTS OF PROCESS VARIABLES ON THE MECHANICAL AND PHYSICAL PROPERTIES OF AN Al-Cu-Mg POWDER METALLURGY ALLOY

by

Bryce Christensen

Submitted in partial fulfilment of the requirements
for the degree of Master of Applied Science

at

Dalhousie University
Halifax, Nova Scotia
April 2018

Table of Contents

List of Tables

List of Figures

Abstract

The applications of aluminum powder metallurgy (PM) alloys require precise control of final mechanical properties. The final properties of an alloy are dictated by the processing steps performed during production. The goal of this research was to analyze the effects process variables have on the properties of Al-2.3Cu-1.5Mg-0.5Sn. Specifically, the impact of heat treatment and sizing on the tensile and fatigue properties was investigated. Three variations in heat treatment were explored, each in the sized and not-sized condition: naturally aged (T1/T2) , artificially aged (T6/T8), and solutionized-naturally aged (T4/T3). Uniaxial tensile testing was done to determine yield strength and ductility. 3-point bend fatigue using the staircase method was used to determine fatigue strength. For all heat treatments, sizing increased yield strength, but decreased ductility and fatigue strength. The T8 heat treatment resulted in the highest yield strength (325 MPa), but also the lowest fatigue strength (109 MPa). The T4 heat treatment resulted in the highest ductility (14%). Sizing decreased fatigue strength by up to 31% in the artificially aged samples. Delay time between sintering and sizing was investigated and no significant impact was seen in mechanical properties by increasing delay time. Differential scanning calorimetry (DSC) was used to determine if sizing impacted precipitate development. It was determined that the precipitation sequence of the S-type (Al_2CuMg) was influenced by sizing. Through the DSC data it was inferred that there was a preferential tendency for S1-type precipitates to form in sized samples, supressing full aging to S2-type. This would have altered the mechanical performance of the alloy.

List of Abbreviations and Symbols Used

PM: Powder Metallurgy

OAL: Overall Length

DWF: Die Wall Friction

LPS: Liquid Phase Sintering

E-C: Evaporation-Condensation

GB: Grain Boundary

UTS: Ultimate Tensile Strength

YS: Yield Strength

σ: Stress

μ: Coefficient of Friction

Acknowledgements

The author would like to acknowledge the Natural Sciences and Engineering Research Council of Canada (NSERC) for financial support via the Collaborative Research & Development grant CRDPJ 486528 - 15. Dr. Bernhard Mais (Kymera International) is gratefully acknowledged for the provision of the powdered metals employed, while Mr. Randy Cooke, Dean Grijm, and Mark MacDonald are thanked for technical assistance.

Chapter 1.0 Introduction

Powder metallurgy (PM) is an incredibly diverse and useful method of metal and composite part production. Industrial use of PM is growing at a considerable rate as it becomes more economical to produce reliable parts. There are many advantages to PM including:

- Near net shape processing
- High volume production capabilities
- Low cost/part at high production rates

In recent years, the use of aluminum PM has been growing in areas such as automotive manufacturing, as there is a strong push to create lightweight replacement parts for ferrous alloys. Aluminum PM parts have been successfully implemented in automotive applications such as camshaft bearing caps and transmission carrier assemblies. As manufacturers look to reduce weight, aluminum PM alloys are beginning to be implemented more frequently. There are many different methods of PM production ranging from conventional press-and-sinter PM to spark plasma sintering (SPS). The former typically uses rigid dies and tooling to compact metal powders into green bodies which are then sintered to bond the powder particles together and improve mechanical properties. After sintering, secondary operations such as sizing and machining can be performed to completely finish the part. Sizing is a re-striking of the sintered part which is used to meet final dimensional tolerances. This conventional press-and-sinter PM approach is efficient, but is currently limited to relatively small parts (hand sized).

Despite this size limitation, conventional PM is a widely used processing method. Aluminum alloys are good candidates for conventional PM because of their relative soft nature, which allows for higher densification at lower compaction pressures [1]. Conventional PM typically the follows the basic stages of:

1. Powder production and mixing
2. Die compaction
3. Sintering
4. Secondary operations

A common secondary operation for aluminum PM parts is sizing; which is used to control final dimensional tolerances. Sizing involves applying a load to sintered parts which reduces the overall length (OAL) via cold work. Another common secondary operation is heat treatment. Many aluminum alloys are strengthened mainly through precipitates; the type and number of precipitates depends mainly on alloy chemistry and the processing parameters employed during heat treatment. Different heat treatment processes can have various impacts on mechanical properties in aluminum alloys [2]. The impact of secondary operations (specifically heat treatment and sizing) on the mechanical and physical properties of 2xxx series aluminum alloys will be discussed in detail later.

1.1 Powder Production and Mixing

There are many different powder production methods available, each of which has its own benefits. In the context of press-and-sinter PM, the aluminum powder is usually produced by gas atomization [4]. Here, the metal/alloy of interest is melted and then

allowed to flow from the crucible as a thin, continuous stream. Jets of high pressure gas then impinge on the stream and disrupt it into a mist of fine droplets that eventually solidify into discrete powder particles as they travel down through the atomization chamber. Air is often the gas of choice, but inert gases can be used when control of the oxygen content is necessary. Figure 1 shows the gas atomization process. Various controls can be manipulated to influence powder morphology and size distribution including melt temperature, nozzle geometry, velocity of the gas and/or metal, and gas pressure[3].

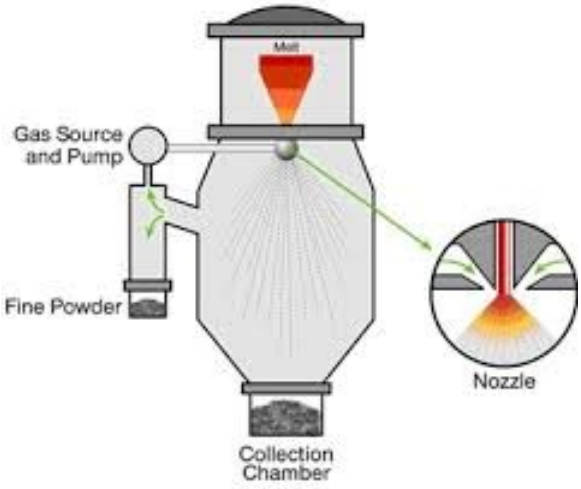

Figure 1. Schematic of the gas atomization process [5].

Once the powder has been fabricated, it is then blended with other powders to create the desired alloy composition. It's rare that only one single elemental powder is used for PM, usually multiple powders must be mixed together to form a homogenous powder blend. These powders can be elemental or pre-alloyed. Lubricant can also be added at this stage. Lubrication is necessary to reduce friction during compaction. If it is not added during mixing, lubricant must be added to the die prior to compaction. At high scale production

levels, it is often easier to add lubricant to the powder blend, rather than lubricating the die before every compaction cycle. Once the proper powders and lubricant have been mixed, they are ready for compaction.

1.2 Die Compaction

Die compaction is the first step in powder consolidation. Here, the loose powder mixture is typically consolidated by means of uniaxial die compaction (i.e. the pressing direction is along a single vertical axis). The product is referred to as a "green body" which has the consistency of chalk, but a geometry that closely approximates that of the intended final product. Four typical stages occur during die compaction:

1. Rearrangement
2. Localized deformation
3. Homogenous deformation
4. Bulk compression

Rearrangement occurs at the lowest compaction pressures, whereas bulk compression occurs only at the highest compaction pressures. The four stages of compaction and the relative green density they produce are illustrated in Figure 2.

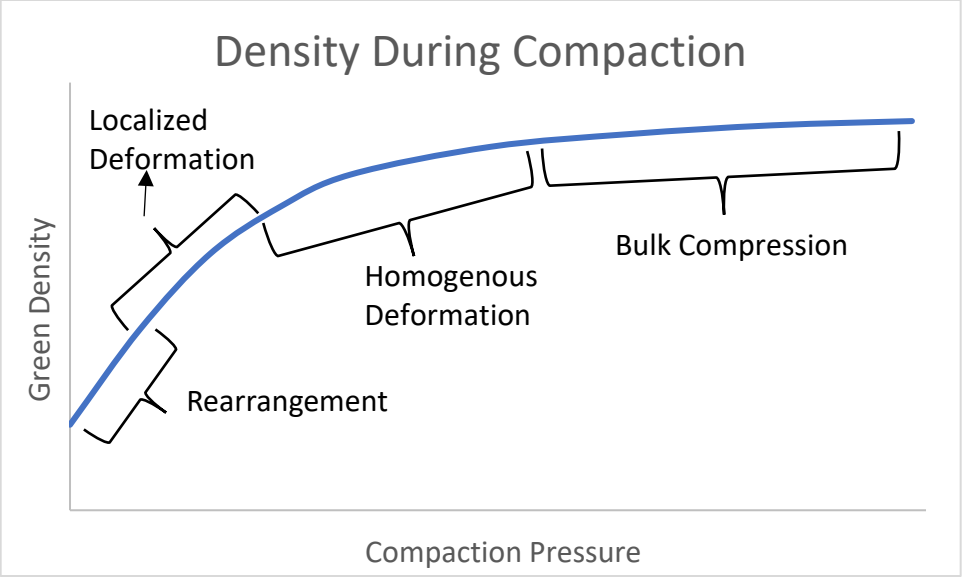

Figure 2: Green density vs compaction pressure with stages of compaction labelled.

During rearrangement, densification occurs due to the particles shifting their positions to fill larger voids. Particle deformation begins during the next stage - localized deformation. Here, the point contacts between particles begin to deform to produce larger areas of contact. This promotes a more efficient packing arrangement and thereby increases green density further. During the subsequent stage of homogenous deformation, the point contact deformation spreads through the entire particle. Densification continues but the extent of increase becomes subdued owing to the fact that the entire volume of most particles is now heavily work hardened. The final stage of the compaction sequence is bulk compression. At this point, the particles are work hardened and only small pores remain. This scenario mandates the application of very high pressures to realize even small gains in green density. For this reason, it is generally impractical to utilize a compaction pressure that will manifest bulk compression. A reasonably high percentage of the theoretical density can generally be realized by

compacting into the homogenous deformation stage and this is typically viewed as the upper limit for die compaction.

Punches and dies are used to compact the powder. The number of punches required depends on the complexity of the part and the desired green density. For this reason, parts are classified depending on the number of levels and the number of pressing directions (one or two). Table 1 shows the different part classifications.

Table 1: PM part classifications based on number of levels and pressing directions.

Part Class	Number of Levels	Pressing Directions
1	One	One
2	One	Two
3	Two	Two
4	Several	Two

It is important to note that "single action" indicates one pressing direction and "double action" indicates two pressing directions (top and bottom concurrently). The difference between the two is of significance because each will produce a compact of different green density uniformity. A double action press will produce a compact with less variation in density. This means there will be a more uniform density throughout the part, resulting in better mechanical properties in the final product. Single and double action presses are

displayed in Figure 3. Examples of the density gradients each pressing action produces are shown in Figure 4.

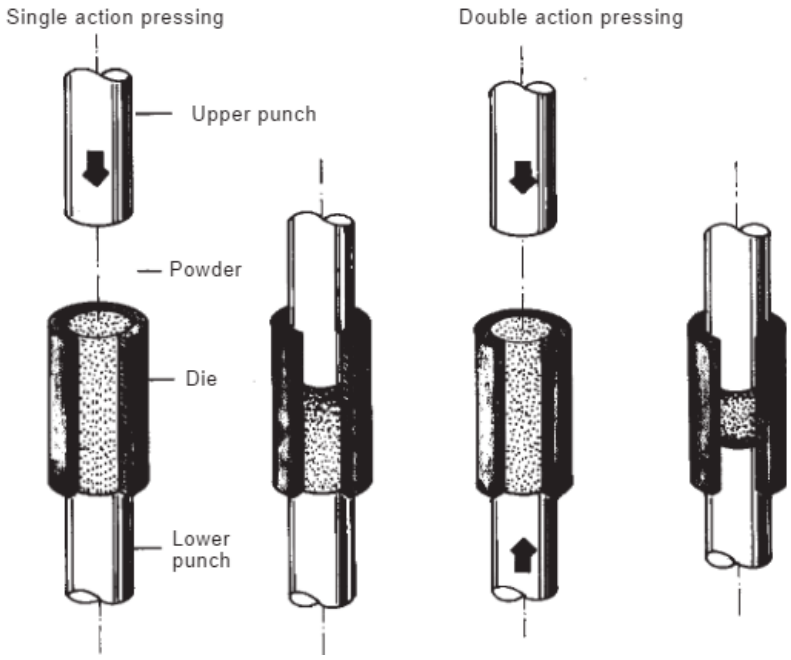

Figure 3: Diagrams of single action (left) and double action (right) compaction [3].

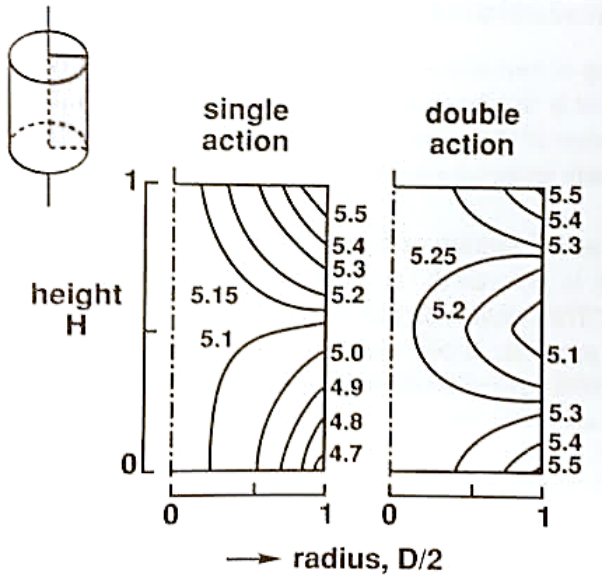

Figure 4: Density gradients created in single and double action compaction [1].

Both single action and double action compaction will produce density gradients within the compact; however, the density variation in the double action compact is reduced relative to that resulting from single action [1]. For a single action press, the density will decrease with greater distance from the upper punch. For a double action press, the area in the middle of the compact is the least dense since both the upper and lower punches transmit pressure to the compact. This location is known as the "density split".

The reason why density variation occurs during compaction is due to die wall friction (DWF). Because of DWF, pressure applied at the compact's surface is not transmitted all the way through the compact. Lubrication can reduce DWF, but cannot completely remove its effects. The effects of DWF can be quantified in terms of the applied compaction pressure within a simple cylindrical compact using the following equation:

$$P_x = Pexp\left(-\frac{4\mu zx}{D}\right)$$

Where: P_x – Pressure at distance x
P - Applied pressure
μ - Coefficient of friction
z - Proportionality constant
x – Distance from punch
D - Diameter

DWF is a major issue encountered during die compaction and must be partially mitigated with the addition of lubrication. In doing so, the coefficient of friction can be reduced resulting in a more uniform green density, lower ejection forces, and improved tooling life [1]. Though the addition of lubrication is necessary, the selection of an appropriate

amount is essential as excessive concentrations can decrease apparent density and, potentially, the final density of a green compact.

For successful die compaction to occur, powder with the correct characteristics must be utilized. Powder attributes that have a particularly significant effect on compressibility include particle size, morphology and chemistry [1]. Smaller particles require more energy to compress because they invariably impart an abundance of smaller pores. These small pores are difficult to eliminate due to a high coordination number (high number of particle contacts). In the case of particle morphology, irregular but rounded particles are typically preferred as these often result in higher green strengths due to an increase in particle interlocking. Particle chemistry is also important during compaction because powders that contain pre-alloyed additions have higher yield strengths than pure (i.e. elemental) counterparts. Hence, pre-alloyed powders typically require appreciably higher compaction pressures and suffer from inferior green strength.

1.3 Sintering

Sintering is principally responsible for the development of acceptable mechanical properties in the final product [6]. Fundamentally, this stage seeks to establish appropriate metallurgical bonding between powder particles at high temperatures. The powder compact attempts to reduce its energy by lowering its overall surface area through different mass transport mechanisms [1]. There are multiple different types of sintering, but the most important type for aluminum alloys is liquid phase sintering (LPS). Small

amounts of solid-state sintering also occur prior to LPS, so it is important to have a basic understanding of the underlying mechanisms for solid state in addition to LPS.

Considering solid state sintering first, there are five mass transport mechanisms that can occur. They are split into surface transport (movement of surface atoms) and bulk transport (movement of bulk atoms) as follows:

Surface Transport:

- Evaporation-condensation
- Surface diffusion
- Volume diffusion

Bulk Transport:

- Grain boundary diffusion
- Volume diffusion

To explain these five mechanisms, it is helpful to use a two-sphere model. This model is a simple representation of two particles connected by a neck, as shown in Figure 5.

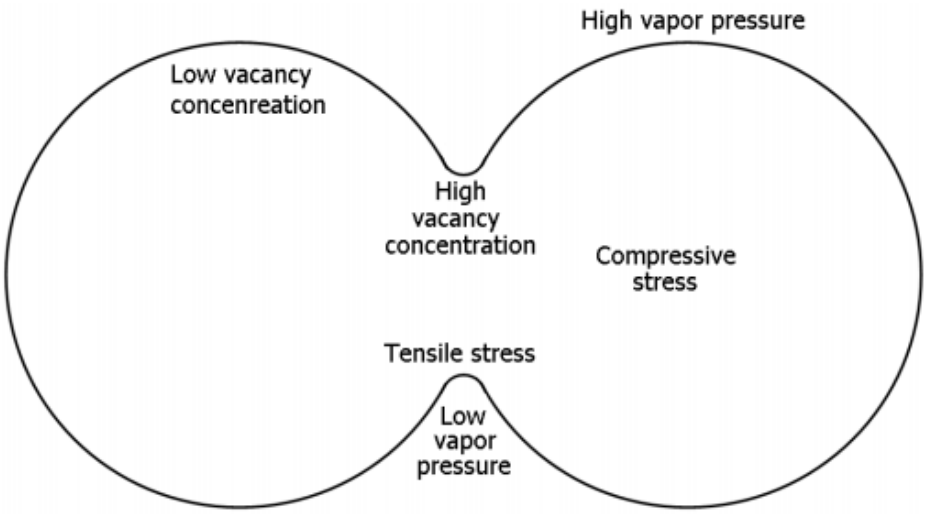

Figure 5: Two sphere particle model with various conditions labelled [7].

Evaporation-condensation (E-C) occurs because of a pressure gradient which forms between the neck and the particle bulk. Here, an area of low vapour pressure forms at the concave neck while an appreciably higher vapour pressure forms along the convex particle surface. The system then attempts to eliminate this pressure differential by the transport of vapour into the neck region. Because the neck remains concave, this movement of mass over-pressurizes the region. To restore equilibrium, vapour then condenses on the neck thereby depositing material and causing particle bonding [1]. E-C occurs at the lowest sintering temperatures of all the mass transport mechanisms.

As temperature is increased, surface diffusion will occur; driven by gradients in the concentrations of surface vacancies. At the neck, the concentration of this feature is high, but at the convex particle surface it is proportionately lower. Hence, a vacancy migration away from the neck occurs along the surface, causing a counter-current flux of surface atoms to diffuse towards the neck. This shifts mass into the inter-particle contact which

causes the neck to grow. Surface transport volume diffusion is underpinned by the same concept, but now the path for the diffusion of the atoms that originate at a surface is through the interior of the particle and not exclusively along a free surface. This particular means of mass transport becomes more effective at higher temperatures owing to a synergy between the increased number of pathways available and more rapid rates of diffusion [1].

Grain boundary (GB) diffusion leads to densification in part because of a grain boundary that forms at the neck. Grain boundaries are highly disordered regions where diffusion rates are rapid and vacancy annihilation can occur. This annihilation leads to overall densification of the compact. Bulk transport volume diffusion is driven by a vacancy gradient between the bulk of the particle and the neck. As the name indicates, atom diffusion is through the bulk volume of the particle.

The five mechanisms described above occur at different temperature regimes. These rank as follows:

$$T_{E-C} < T_{S.D.} < T_{V.D.surface} < T_{GBD} < T_{V.D.bulk}$$

As the mechanisms of solid state sintering transpire, three stages commensurate with observable changes in the microstructure occur: initial stage, intermediate stage, and final stage. The stages progress with increased temperature and time. During the initial stage, neck growth takes place, but minimal densification occurs. The pores become slightly rounded, but for the most part remain irregular. The main driver of these changes is E-C

and surface diffusion arising from curvature differences. During the intermediate stage, pores become very rounded, densification begins, and grain growth occurs. The driving force during this stage is the reduction of surface area/energy through pore structure changes [1]. The final stage is much slower than the first two and for this reason, final stage sintering is infrequently achieved in the PM industry. During the final stage there is a surge in grain growth and the pores become spherical. Here, pores can break away from these boundaries at prolonged sintering times so as to become isolated within the bulk interior of a grain. When this occurs, densification is effectively discontinued.

Diffusion rates are very important during sintering. The faster diffusion can occur, the better the sintering response will be. Diffusion occurs at much higher rates in liquid metal than in solid metal, so there are significant advantages to having liquid present during sintering. However, additional factors must also be considered for a particular alloy is to be amenable to LPS:

- High solubility of solid in liquid
- Low solubility of liquid in solid
- Wetting of the liquid on the solid grains

Figure 6 shows an alloy system with these key requirements, along with some other ideal features for LPS. The high solubility of B in A means requirement 1 is met. The low solubility of A in B means requirement 2 is met. In addition, there is a large melting difference between A and B which is a beneficial feature for LPS. For LPS to occur, the

alloy is heated to just above the solidus line to the point on the figure marked “liquid phase”.

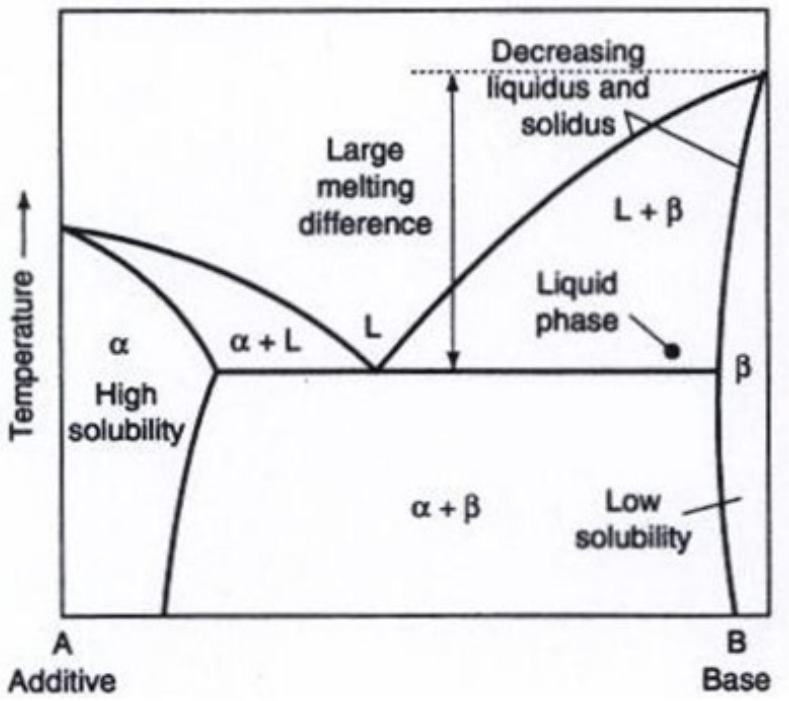

Figure 6: Phase diagram for an ideal base-additive system for LPS [8].

Similar to solid-state sintering, LPS also transpires through a series of different stages:

1. Heating
2. Rearrangement
3. Solution-reprecipitation
4. Final stage

Figure 7 shows the different stages of LPS. Note that the heating stage is labelled as “solid state” in Figure 7.

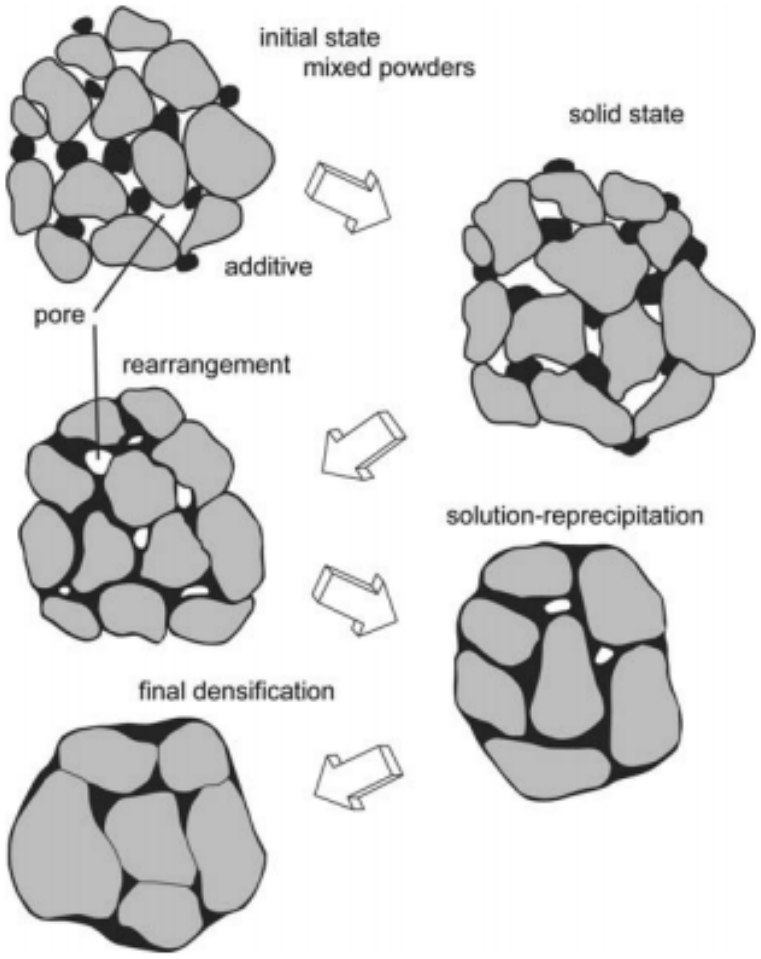

Figure 7: Schematic of the stages of liquid phase sintering [9].

During the heating stage, the metals remains solid and a mild degree of solid-state sintering occurs. Once liquid begins to form, rearrangement starts. During rearrangement, rapid densification occurs via the flow of liquid metal into the open pores; this is commonly termed "densification burst". The liquid is drawn into the pores through a combination of wetting and capillary draw [1], hence why this is one of the key requirements for LPS. During solution-reprecipitation, the grains begin to grow through Ostwald ripening which is the growth of large grains at the expense of smaller grains. Because of the liquid present, diffusion of the base metal from small to large grains can

occur faster than in solid-state sintering. Once the final stage is reached, there are mild (if any) density gains which require extended sintering periods. The grains continue to grow in the final stage.

The biggest advantage of LPS is faster sintering rates [10]. Other benefits include: grain size control, rapid compact densification through capillary draw, and liquid dissolution of sharp edges on particles which results in better packing[10]. The major drawback of LPS is compact distortion (often called compact slumping) [10]. Compact slumping occurs when too much liquid is formed during the sintering process; therefore, it is important to control the amount of liquid present in a given system. Typically, in systems such as Al-Cu, a liquid fraction of around 15% is targeted[11]. This liquid fraction promotes optimal sintering, without significant slumping occurring. For an Al-Cu alloy such as AA2014, θ-phase eutectic is formed when the temperature is higher than the eutectic temperature of 548°C [12]. The formation of this eutectic melt triggers liquid phase sintering. Liquid phase sintering of the Al-Cu system is discussed further in section 1.5.1.

In addition to the core stages discussed above, the nature of the oxide film present on the powder particles also plays an important role. In the case of aluminum powder, it has been determined that this exterior film is primarily alumina (Al_2O_3) [6, 13-15] which is amorphous and hydrated [6]. This phase has exceptionally high thermodynamic stability. For instance, to reduce aluminum in a conventional atmosphere (i.e. one that contains a reducing gas such as hydrogen), either a dew point below -140˚C or an oxygen partial

pressure (P_{O2}) less than 10^{-50} atm is required [6]. Neither of these requirements are attainable, so this layer must be physically disrupted by some means if inter-particle diffusion and, in turn, sintering is to transpire. Adding magnesium is an effective way to remedy this problem. Here, the magnesium reacts with alumina to form spinel ($MgAl_2O_4$) according to the following reaction:

$$3Mg + Al_2O_3 \leftrightarrow 3MgAl_2O_4 + 2Al \qquad [16]$$

The formation of spinel disrupts the oxide layer through following steps [16]:

1. Al-Mg contact sites are formed during compaction which instills small, localized fractures in the oxide layer.
2. Magnesium diffuses through aluminum and along metal-oxide interfaces.
3. Magnesium reduces the oxide at this interface, forming spinel.
4. Aluminum particles which are not directly in contact with the Mg are subsequently exposed to the reductant, causing disruption of their oxide layers.

Once magnesium has disrupted the oxide layer, conventional LPS mechanisms can then engage to consolidate the aluminum PM compact and thereby enhance metallurgical integrity. The addition of other elements can also increase sintering response for aluminum, resulting in a final product with better properties. Other PM alloying additions are explored in 1.5.

One of the most important aspects to consider when sintering aluminum is the surrounding atmosphere. Aluminum can easily oxidize further under inappropriate conditions, so at the very least, the sintering atmosphere should limit further oxidation. Oxygen concentration and the dew point are key parameters that will limit this effect. These are generally held to <10ppm and <-50°C respectively in commercial practice. Amongst the different atmospheres available, nitrogen is generally regarded as the best. Not only does it limit any further oxidation, but can actually induce pore filling through the *in-situ* formation of aluminum nitride. When aluminum nitride is formed, the pressure inside the pore is reduced leading to unbalanced internal and external forces [17]. To restore balance, even the largest pores will fill leading to an increase in overall density.

1.4 Secondary Operations

Secondary operations are commonly performed on sintered PM parts to enhance dimensional accuracy, value, and performance. These operations can include: sizing, heat treatment, resin impregnation, and machining. Of these, heat treatment and sizing are particularly common for aluminum PM alloys. Various thermal heat treat treatments for aluminum alloys are shown in Table 2. Each will impact the mechanical properties of an aluminum alloy differently.

Table 2. Commonly utilized thermal heat treatments for aluminum alloys [18].

Temper Designation	Sequence of Events
T1	1. Cooled from elevated temperature 2. Naturally aged
T2	1. Cooled from elevated temperature 2. Cold worked 3. Naturally aged
T3	1. Solution heat treated 2. Cold worked 3. Naturally aged
T4	1. Solution heat treated 2. Naturally aged
T5	1. Cooled from elevated temperature 2. Artificially aged
T6	1. Solution heat treated 2. Artificially aged
T7	1. Solution heat treated 2. Artificially aged
T8	1. Solution heat treated 2. Cold worked 3. Artificially aged
T9	1. Solution heat treated 2. Artificially aged 3. Cold worked
T10	1. Cooled from elevated temperature 2. Cold worked 3. Artificially aged

Sizing is primarily utilized to ensure each part is within dimensional tolerance but this operation can also alter the properties of the finished product. For example, the corrosion rate of the 2xxx series PM alloy Alumix 123 is significantly decreased when the alloy is in the sized condition [19]. Since sizing is essentially a form of cold working, it can also have an impact on the mechanical properties of aluminum alloys. In one study it was demonstrated that yield strength and UTS increased significantly when sizing was implemented [20]. Other secondary operations may be necessary to finish PM parts such as machining and resin impregnation. Machining is common in industry since features such

as threaded holes cannot be introduced into the part during compaction whereas resin impregnation is implemented to seal off residual porosity and yield a pressure-tight part.

1.5 Overview of Al-Cu-Mg PM Alloy Systems

In many instances, commercial aluminum PM alloys are premised on the Al-Cu-Mg ternary; in essence, the 2xxx series. When the correct amounts of Cu and Mg are added, these alloys exhibit a good response to compaction and sintering. Small amounts of other elements (such as tin and silicon) can be added to further enhance select attributes.

1.5.1 Role of Copper and Magnesium

Copper is commonly alloyed with aluminum in wrought, cast, and PM alloys. Al-Cu systems are strengthened by precipitation hardening which occurs via heat treatment. In PM, copper also plays a critical role processing as it influences how much liquid will be present during sintering at a specific temperature [11]. Figure 8 shows how copper concentration affects the amount of liquid phase present in the PM alloy AC2014. For aluminum PM, a liquid fraction of 10-20 wt% is generally targeted in sintering as it often strikes an appropriate balance between densification and distortion [11]. This range is shown as the shaded areas in Figure 8 for each copper concentration considered. It is apparent that copper enables the attenuation of an acceptable concentration of liquid phase, and that the desired range for sintering shifts to lower temperatures and broadens slightly as the concentration of this element increases. As such, copper is an effective

addition in aluminum PM systems as it is critical to processing (liquid phase sintering) and the mechanical properties of the finished product (precipitate strengthening).

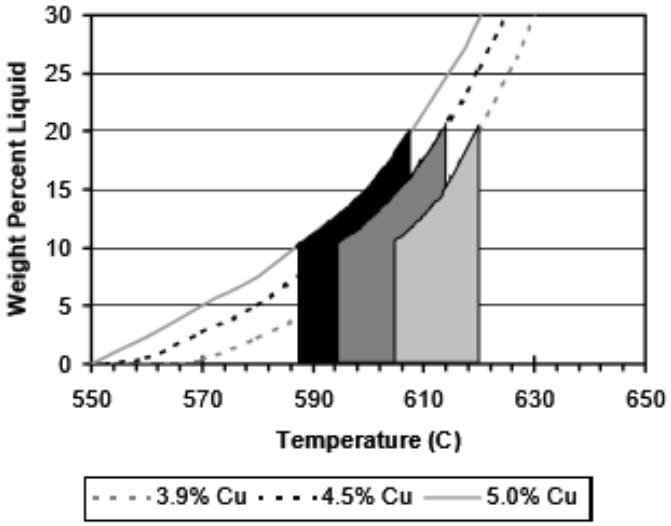

Figure 8: Effect of Cu on liquid content for AC2014 at increasing temperatures [11].

Copper is often incorporated into the powdered feedstock as master alloy powder mixed with elemental aluminum. During compaction, the soft aluminum particles will deform around the harder Al-Cu particles. As the master alloy content is increased, a higher fraction of the Al-Cu particles will be in contact with themselves to the detriment of green strength. However, the use of a master alloy (i.e. Al-50Cu weight %), as opposed to a mixture of elemental copper and aluminum powders, is known to impart an intensified sintering response and concomitantly, a product that exhibits near full density and excellent mechanical properties [21]. Hence, while care must be exercised with this approach in compaction, such concerns are readily offset by the metallurgical attributes of the high-quality product.

The role magnesium plays in the sintering of aluminum PM systems was previously discussed in section 1.3. The disruption of the aluminum oxide layer by spinel ($MgAl_2O_4$) formation is very important in aluminum PM systems, including Al-Cu-Mg alloys. However, magnesium also forms a strengthening precipitate with aluminum and copper; this and other precipitates are discussed in the following section.

1.5.2 Precipitate Strengthening in Al-Cu-Mg

In Al-Cu-Mg PM alloys, strengthening typically comes from two main precipitates: θ-type ($CuAl_2$) and S-type (Al_2CuMg) [2]. Both can be present in Al-Cu-Mg systems, but the chemistry and processing parameters dictate which precipitate will be dominant. For example, AC2014 is strengthened primarily by θ-type precipitates, whereas PM2324 is strengthened by a combination of the two [20]. S-type precipitates have an orthorhombic Cmcm structure with lattice parameters of a_s = 0.400 nm, b_s = 0.923 nm, c_s = 0.714 nm[22]. The structure of θ-type precipitates is typically described as condensed tetragonal antiprisms along [001] [23]. The amount of each precipitate present can be influenced by temperature as demonstrated by the thermodynamic calculations presented for PM2324 in Figure 9. As temperature increases, the weight fraction of θ increases to the point where it surpasses S near 200°C. As the temperature increases above 500°C, both S and θ-type precipitates are no longer stable.

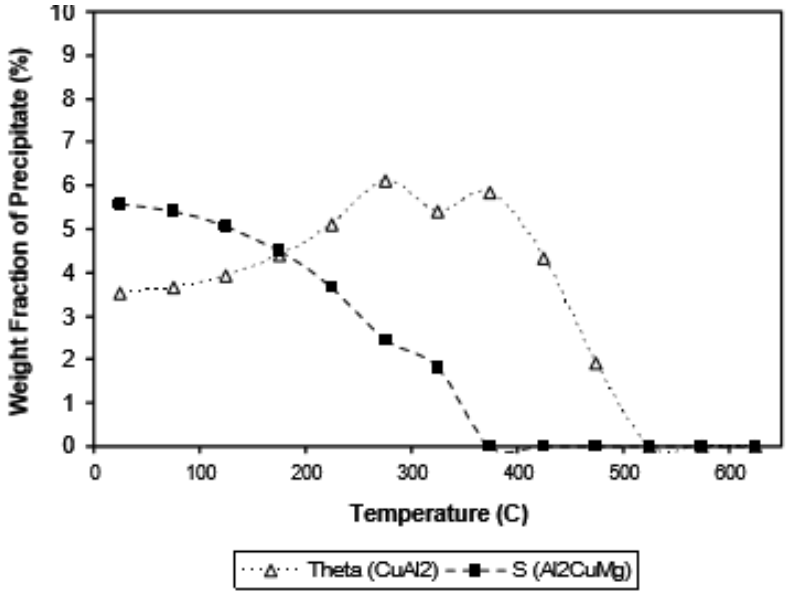

Figure 9: Thermodynamic calculations predicting the precipitate phases present in PM2324 as a function of temperature [20].

Preferred nucleation site is a key difference between S-type and θ-type precipitates in that the former tend to nucleate on dislocations, whereas the latter do not. It is for this reason that alloys strengthened primarily by S-type precipitates are often cold worked prior to aging. Cold work generates additional dislocations within the microstructure, leading to a high concentration of nucleation sites for S-type precipitates. The aluminum PM process often involves sizing (cold work) prior to aging. Hence, it is advantageous to select an alloy chemistry which is primarily strengthened by S-type precipitates so as to realize a refined distribution of precipitates and enhanced mechanical properties [2].

Alteration of the Cu:Mg ratio is an effective way to control the dominant precipitate present. In this sense, a low value will favour S-type precipitates whereas a high value

will yield an alloy predominately strengthened by θ-type precipitates [2]. Hence, if the Cu:Mg ratio can be lowered but maintain good compaction and sintering characteristics, it can be advantageous to do so for aluminum PM production cycles that involve sizing. Cooke et al. [2] studied one such alloy - Al-2.3Cu-1.6Mg, which has a Cu/Mg ratio of 1.44:1. Figure 10 and 11 show the compaction and sintering curves for this system. It is evident that the alloy compacted well, having reached green densities > 95% of theoretical at a compaction pressure of ~400 MPa. A desirable sintering response was also noted as final densities >98% of full theoretical were realized.

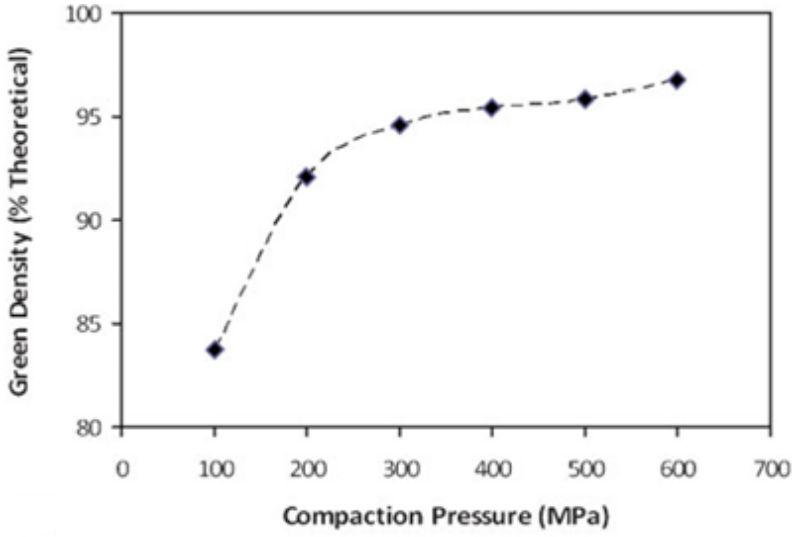

Figure 10: Green density as a function of compaction pressure of Al-2.3Cu-1.6Mg [2].

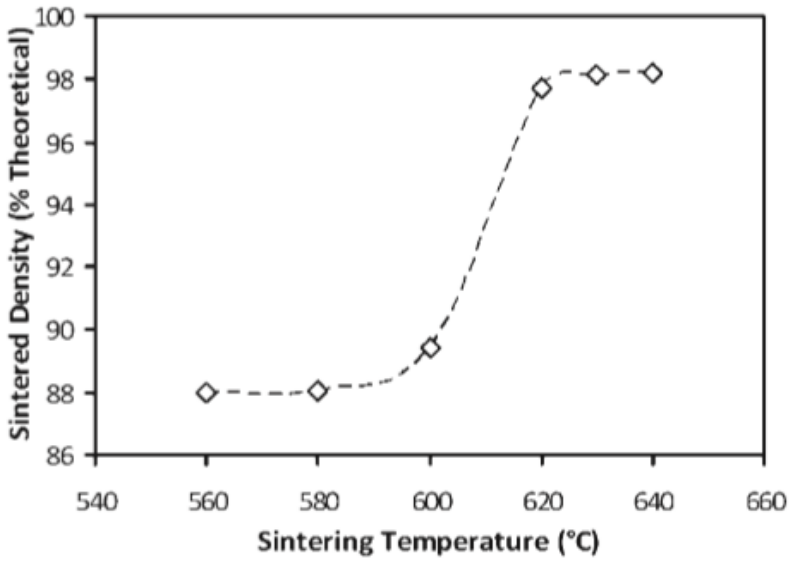

Figure 11: Sintered density of Al-2.3Cu-1.6Mg as a function of sintering temperature [2]

Prior studies have shown that the concepts discovered for wrought and cast alloys are largely consistent with those noted for PM alloys. For example, the commercial PM alloy AC2014 (Al-4.5Cu-0.6Mg-0.8Si) has a Cu:Mg ratio of ~9:1 which would imply a high fraction of θ precipitates. TEM observations on this alloy have confirmed that this is in fact the case [24].

When targeting aluminum PM alloys that rely on S-type precipitates, it is insightful to consider the underlying precipitation sequence; a topic that has been debated over the years. Initially, it was proposed that the precipitation of the S phase was as follows [25]:

$$SSS \rightarrow GPB\ Zone \rightarrow S'' \,/\, GPB2 \rightarrow S' \rightarrow S$$

Here, SSS indicates a supersaturated solid solution. This stage exists directly after water quenching and represents a scenario wherein copper and magnesium are dissolved in the α-aluminum grains at concentrations beyond their equilibrium values. When this metastable phase begins to decompose, GPB (Guinier-Preston-Bagaryatsky) zones are initially formed. GPB zones are sub-nanometer sized phases that have rod-like structures [26]. The formation of GPB zones signals the initiation of precipitate generation. In recent years, the formation of Cu-Mg co-clusters have often been inserted into the precipitation sequence before GPB1 zone formation; sometimes as a substitution for GPB1 zones. Generally, it was accepted that the S' phase was semi-coherent with the matrix and the S phase was incoherent with the matrix [27]. Later, a change to the sequence was proposed by Wang and Starink [27] that suggested a slightly different variation:

$$SSS \rightarrow Clusters \rightarrow S" \,/\, GPB2 \rightarrow S(Type\ I) \rightarrow S(Type\ II)$$

The main difference being that the S(type I) and S(type 2) are crystallographic variations of the S phase. Although type II is more stable, actions such as cold working can supress its formation and lead to an increased concentration of its metastable precursor (type I). The transformation from type I to type II has been reportedly documented via DSC in some instances. Figure 12 shows DSC testing done by Parel et al. [28] on cold worked and quenched samples of wrought Al2024. In the "quench only" sample a small shoulder effect is seen in the main peak at 290°C. This effect is believed to be the transformation of S(type I) to S(type II). Note that a similar peak was not observed in either of the cold worked samples as this is known to supresses the transformation.

The thermal flux coincident with the type I to type II transformation is quite small, as only strain energy and interfacial energy are released during the subtle transition [27]. However, in select instances it has reportedly led to distinct peaks in the DSC trace, as demonstrated in Figure 13. Here, discrete peaks corresponding to type I and type II (labelled CI and CII, respectively) were observed. The existence of two distinct variants was then confirmed by direct observation via TEM [27].

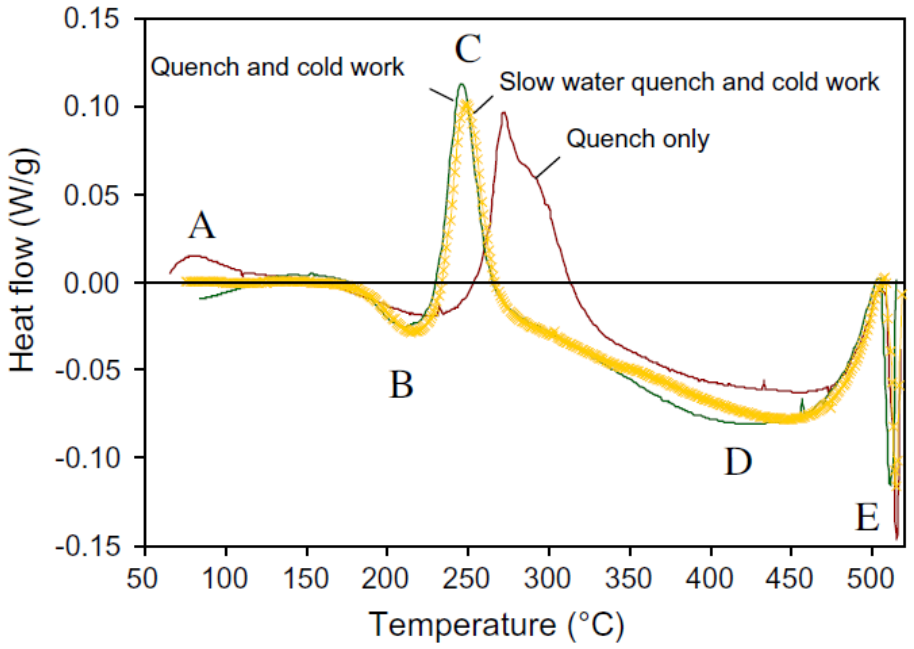

Figure 12. DSC traces acquired from samples of wrought Al2024 after different precursory treatments [28].

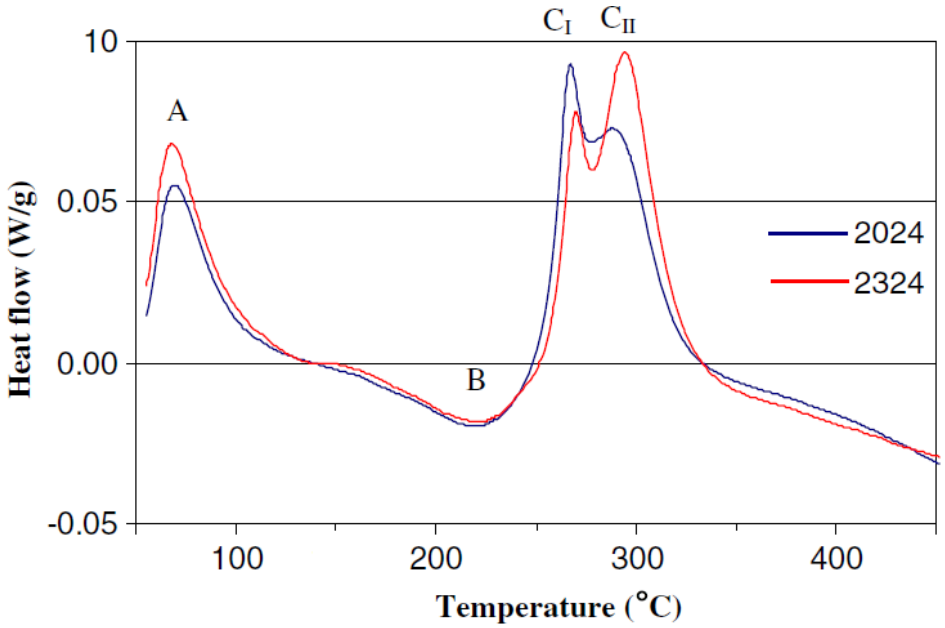

Figure 13. DSC traces acquired from samples of wrought alloys Al2024 and Al2324 directly after quenching in water [27].

1.5.3 Tin and Silicon Alloying Additions

The sintering response of aluminum PM alloys can be improved by the addition of other elements such as silicon and tin [2, 20, 29]. In the case of tin, small additions create an increase in sintered density and therefore, sintered strength. This increase occurs because tin limits the nitridation of liquid aluminum during sintering [29]. When tin is not present, a nitride layer can form on the surface of liquid aluminum, negatively affecting liquid phase wetting ability [29]. Although small amounts of tin are beneficial to the sintering of Al-Cu-Mg alloys, excessive amounts can have a negative effect. This is illustrated in Figure 14 and 15 which show the effect of tin content on sintered density and strength, respectively, for an Al-Cu-Mg PM alloy. Here, the sintered density reached a peak at 0.5 wt% tin and then began to decrease as the tin content was increased. Similarly, UTS and

yield strength peaked at 0.2 wt% and then declined. It has been postulated that the declines occur because tin acts as a scavenger for magnesium, effectively increasing the Cu:Mg ratio. At low tin concentrations, the scavenging effect is minimal and is offset by the gains accrued through controlled nitridation. However, tin contents in excess of that required for nitridation control can increase the Cu:Mg ratio and therefore suppress the formation of (S-type) precipitates [20] to the detriment of mechanical properties.

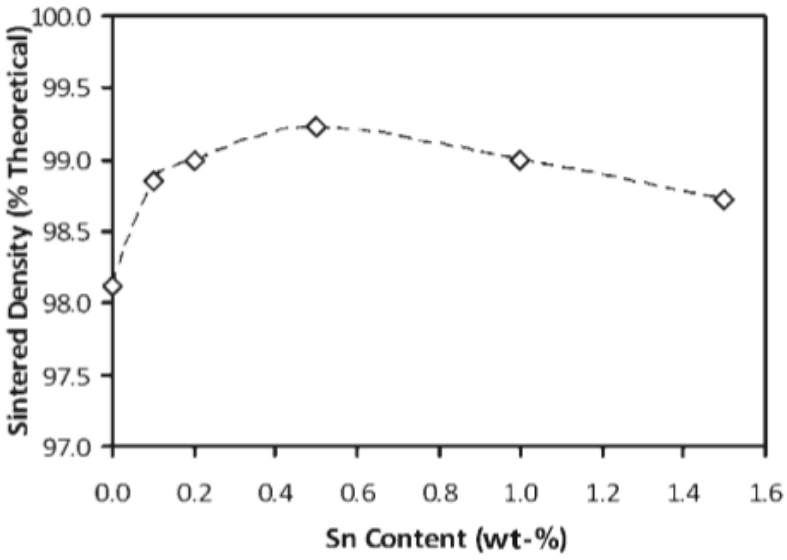

Figure 14: Effect of tin content on the sintered density of Al-2.3Cu-1.6Mg [2].

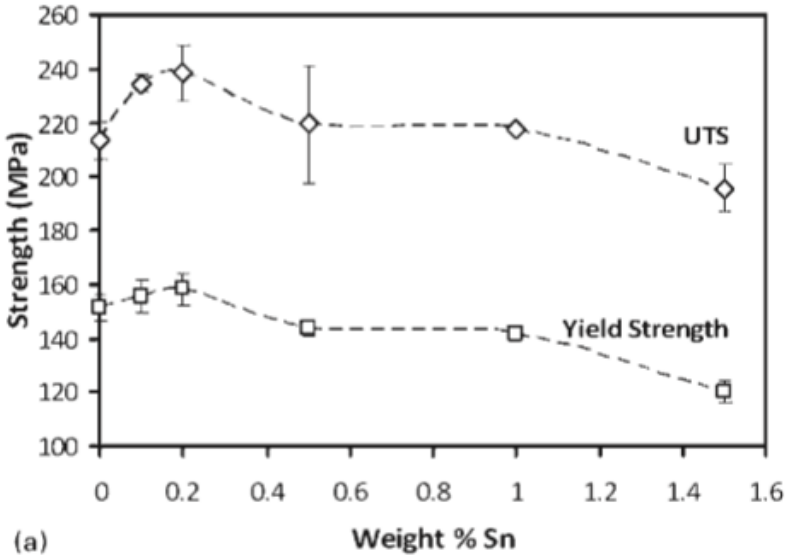

Figure 15: Effect of tin content on the tensile yield strength and UTS of PM Al-2.3Cu-1.6Mg [2].

Similar to tin, silicon additions can also have a positive effect on the final properties of Al-Cu-Mg alloys. During sintering of some Al-Cu-Mg alloys, silicon can increase the amount of liquid present [29]. For example, the addition of 0.7 wt% Si to Al-3.8Cu-1Mg at 590˚C in argon displayed an increase from 9.2 mol% liquid (no Si) to 16.4 mol% liquid [29]. The increase in liquid content produced an alloy with better sintering characteristics. In other alloys, the beneficial effects of silicon are due to a modification of the precipitates as opposed to an increased sintering response. In one instance of this, Cooke et al. [30] added 0.2 wt% Si to Al-2.3Cu-1.6Mg-1.1Fe-1.0Ni-0.2Sn and observed a significant increase in hardness, YS, and UTS. The silicon addition did not have any advantageous or adverse effects on sintering response, but did prove beneficial during heat treatment. Here it was contended that silicon created subtle changes to the

underlying precipitates (Si-modified GP zones) which lead to the strength increases shown in Table 3. The addition of silicon increased YS by 29% and UTS by 15% making it comparable to the wrought counterpart. The only property that was not increased was ductility, but it remained within the normal range for aluminum PM alloys.

Table 3: Tensile properties for PM2618 with tin and silicon additions [30].

Alloy	*E* (GPa)	YS (MPa)	UTS (MPa)	Ductility (%)
PM2618-Sn	71 ± 2	287 ± 11	351 ± 13	2.7 ± 0.8
PM2618-Sn–0.2Si	70 ± 3	366 ± 7	405 ± 8	1.9 ± 1.1
Wrought 2618	72 ± 2	400 ± 6	456 ± 11	9.2 ± 0.6

1.5.4 Industrial Processing and Sizing of Al-Cu-Mg Alloys

In a growing number of instances, emerging aluminum PM alloys have been successfully, and robustly, processed within industrial production cells [31]. As an example, PM2324 successfully transitioned from laboratory to industry while maintaining or even improving many of its properties [31]. Both compaction and sintering responses were preserved when industrial presses and continuous furnaces were used. Table 4 and 5 compare laboratory and industrial processing of PM2324. Hardness, YS, and UTS all improved in industrial settings; however, this was at the expense of ductility. The increase in hardness and strength were likely due to faster cooling rates in the industrial furnaces.

Table 4: Laboratory vs industrial sintering response of PM2324 [31].

Sintering location	Dimensional change (%)	Mass loss (%)	Density		Hardness (HRE)
			g/cm³	%Theo	
Laboratory	−1.46	1.36	2.68	97.0	86.9
Industry	−1.58	1.39	2.67	96.8	94.6

Table 5: Laboratory vs industrial tensile properties of PM2324 [31].

Sintering location	Yield strength (MPa)	UTS (MPa)	E (GPa)	Elongation (%)
Laboratory	186	248	64.4	1.87
Industry	239	255	60.0	0.89

After sintering, aluminum compacts are often subjected to sizing. This process is used to ensure parts meet dimensional tolerances. Sizing is common in the PM industry to ensure parts are shipped with uniform dimensions. Sizing involves cold working the sintered compact after sintering. An appreciable amount of hardening will occur as a result of sizing, so sizing operations are often performed prior to aging [20]. Sizing does not usually yield fully dense compacts, but can increase mechanical properties mainly by increasing the number of dislocations present. Since an increase in dislocation concentration mostly benefits S-type precipitate nucleation; alloys that are mainly strengthened by S-type precipitates benefit most from sizing.

1.6 Impact of Heat Treatment and Sizing on Properties of Various Alloys Systems

Numerous studies have been done on the impact of heat treatment on the mechanical properties of wrought, cast, and PM aluminum alloys. There are many different papers and handbooks outlining the typical changes in yield strength, ultimate tensile strength, ductility, and fatigue properties of wrought alloys. For example, Table 6 shows the difference natural aging (T4) versus artificial aging (T6) has on the mechanical properties of wrought 2014 (taken from the Smithells Light Metal Handbook [32]). The properties in Table 6 are typical of T4 and T6 tempers, in that T6 alloys usually have higher yield and tensile strengths; whereas T4 alloys usually have higher ductility and fatigue strengths.

Table 6. Mechanical properties of 2014A bar [32].

Temper	0.2% Offset Yield Strength (MPa)	Tensile Strength (MPa)	Elongation (%)	Unnotched Fatigue Strength (MPa)
T4	315	465	17	140
T6	465	500	10	124

There are less available data on the impact of sizing on the mechanical properties of PM alloys. Information on the fatigue behaviour of sized and not-sized PM alloys is especially limited. However, there has been some recent work on the 7xxx series which showed that the fatigue strength of Al-5.6Zn-2.5Mg-1.6Cu could be altered by changing the sizing parameters [33]. Table 7 shows the change in 3-point bend fatigue strength in

sized versus not-sized samples. The fatigue strength decreased by 23% when the alloy was sized after solutionizing, but before aging. It's worth noting that the order of the processing steps was found to have a significant impact on the fatigue strength of the alloy as well. For example, when the same alloy from Table 7 (PM7075) was sized prior to solutionizing, the fatigue strength increased by 5%. This shows that although sizing can negatively impact the fatigue strength of PM7075, if the processing steps are performed in the correct order, the sizing process does not necessarily inhibit fatigue properties.

Table 7. Impact of sizing on fatigue strength of PM7075 [33]

Process	3-Point Fatigue Strength ($\sigma_{50\%}$) MPa
Solutionized-Aged	218
Solutionized-Sized-Aged	168

Chapter 2.0 Research Objectives

The overarching objective of this work was to determine if sizing and heat treatment (or a combination of both) impact the properties of a 2xxx series aluminum PM alloy. Specific interest was placed on how sizing affects the fatigue properties because little is known about this subject. Heat treatment and sizing processes have many variables that can be manipulated such as solutionizing/aging temperatures, aging process, sizing pressures, order of operations, and many others. In this work, emphasis was placed on manipulation of sizing pressures, aging process (natural or artificial), and the time between process steps (sintering and sizing or solutionizing and sizing). The goal was to gain a better understanding of how small changes in processing steps affect the final properties of a 2xxx series aluminum PM alloy.

Chapter 3.0 Effects of Process Variables on the Mechanical and Physical Properties of an Al-Cu-Mg PM Alloy

The research, results, and discussion of the following paper was completed by Bryce Christensen. The co-authors acted as reviewers and editors.

B.D. Christensen[1], D.P. Bishop[1], I.W. Donaldson[2]

1-Dalhousie University, Department of Mechanical Engineering, 5269 Morris Street, Halifax, NS, Canada;
2-GKN Sinter Metals, Advanced Engineering, 2200 N. Opdyke Road, Auburn Hills, MI, USA

Keywords: Aluminum powder metallurgy, Al-Cu-Mg, sizing, fatigue, DSC.

Abstract:

The objective of this research was to analyze the effect sizing and heat treatment had on the properties of a 2xxx series aluminum powder metallurgy (PM) alloy. Al-2.3Cu-1.5Mg-0.5Sn was used for experimental work. Natural and artificial aging was studied, as well as various sizing pressures and delay times between process steps (ex. sintering and sizing). It was determined that sizing increased tensile yield strength but decreased tensile ductility and fatigue resistance. Yield strength increased as much as 32% when sized at 400 MPa, whereas ductility and fatigue strength were reduced by up to 51% and 31%, respectively. Delay time between sintering and sizing (T2 samples) did not appear to significantly impact mechanical properties. Through differential scanning calorimetry (DSC) it was determined that sizing impacted the precipitation of S-type precipitates. It was inferred that there was a preferential tendency for S1-type precipitates to form in sized samples, supressing full aging to S2-type.

3.1 Introduction

Aluminum powder metallurgy (PM) alloys have recently been under intense study due to a push from automotive manufacturers to facilitate reductions in vehicle weight and, in turn, enhance fuel economy. PM is an attractive manufacturing method due to the high volume production capabilities and the reduced need for machining of parts. In particular, 2xxx series aluminum alloys have proven to be viable candidates for automotive PM components due to their effective compaction and sintering responses. The typical processing route for press-and-sinter aluminum PM products includes powder blending, compaction, sintering, sizing, heat treatment and other secondary operations as necessary. A significant amount of recent work has been done on the processing of 2xxx series alloys. Cooke et al. [2] examined the impact of lower Cu/Mg ratios and Schaffer et al. [29] explored the effect of tin and nitrogen on sintering. Other work has studied the industrial processing of Al-Cu-Mg alloys (Boland et al. [31]) or the effect of hot forging on the 2xxx series (Cooke et al. [34]).

Although many of these studies have comprehensively examined various processing methods and the effect of different variables, the impact of sizing has been largely neglected. Specifically, how sizing in combination with various heat treatments affects the mechanical and physical properties of Al-Cu-Mg alloys. This information could be crucial to industrial manufacturers because sizing is essential in commercial aluminum PM production to control final dimensional tolerances. Automotive manufacturers are particularly interested in the impact of sizing on fatigue properties since components can undergo millions of loading cycles in their lifetime. Due to the microstructure (especially

porosity) of PM parts, consistent production methods are necessary to produce consistent fatigue results. Grayson et al. [35] discovered that fatigue cracks in Ampalloy 2712 (Al-3.8Cu-1Mg-0.7Si-0.1Sn) initiated in pores located just below the surface of the material. This highlights the importance of reducing porosity in aluminum PM components.

Sizing is known to change the tensile properties of aluminum PM alloys. Boland et al. [20] found that sizing produced gains in yield strength (YS) and ultimate tensile strength (UTS) while decreasing ductility in an Al-4.5Cu-1.5Mg PM alloy. The gains in YS and UTS were attributed to strain hardening in the material as well as increasing the refinement of S-type precipitates (as discussed in the following paragraph). Although the scope of that study did not include fatigue testing, more recent work on a 7xxx series aluminum alloy has demonstrated significant variations in fatigue strength by altering the sizing parameters [33]. Here, the three-point bending fatigue strength of an Al-5.6Zn-2.5Mg-1.6Cu PM alloy was reduced by 23% when sizing was done immediately after quenching. Harding et al. [33] attributed this decrease in fatigue strength to an increased amount of incoherent η precipitates within the sized microstructures. Here, sizing had altered the solid state reactions that occurred during precipitation hardening and ultimately catalyzed the formation of η precipitates.

2xxx series aluminum alloys are principally strengthened by precipitates. The type and amount of precipitates present in alloys depends on the alloy chemistry and processing route (eg. heat treatment method). Various studies, such as Jena et al. [36], have

determined that S-type (Al_2CuMg) precipitates are prevalent in aluminum alloys with low Cu/Mg ratios. θ-type ($CuAl_2$) precipitates are also common in Al-Cu-Mg alloys, but are more dominant in alloys with a higher Cu/Mg ratio. Cooke et al. [2] found that good tensile properties could be produced by promoting S-type precipitates through a low Cu/Mg ratio in certain PM alloys. Cold working (sizing) is expected to enhance and refine S-type precipitation because this phase is known to nucleate on dislocations [37]. In the present work, an alloy with the composition of Al-2.3Cu-1.5Mg-0.5Sn was studied. This composition equates to a low Cu/Mg ratio of 1.53/1. Hence, S-type precipitates should be the main strengthening mechanism present.

There are various arguments on the how the precipitation sequence of the S phase proceeds. Initially, Bagaryatsky [25] stated the sequence as:

$$SSSS \rightarrow GPB\ zones \rightarrow GPB2\ zones\ (S'') \rightarrow S' \rightarrow S \qquad [R1]$$

Since then, the precipitation sequence has been studied and debated. Wang and Starink [27] proposed that 2 different S-type phases are present and suggested the following precipitation sequence:

$$SSSS \rightarrow Cu - Mg\ Clusters \rightarrow GPB2\ zones\ (S'') \rightarrow S(Type\ 1) \rightarrow S(Type\ 2) \qquad [R2]$$

The S1 type precipitates are metastable and can transform into S2 precipitates depending on processing parameters such as aging time. The precipitation sequence described in

[R2] is generally agreed upon and various researchers (i.e. Styles et al. [38]) have confirmed the presence of S1 and S2 precipitates and that there is a distinct crystallographic difference between them. Given the complexities inherent to precipitation hardening of 2xxx series alloys and the documented influence of cold work/sizing on other aluminum PM alloys, work was completed in this study to determine if similar transitions occurred in a PM alloy of low Cu:Mg ratio and how this impacted fundamental mechanical properties.

3.2 Materials

The PM alloy used in this work was a 2xxx series aluminum alloy with a nominal composition of Al-2.3Cu-1.5Mg-0.5Sn (wt%). The starting powder blend was comprised of air atomized elemental aluminum from Ecka Granules, a 50:50 Al-Cu master alloy, and atomized elemental magnesium and tin powders. The particle size distribution of each powder was measured using laser light scattering (Malvern Mastersizer 3000). A summary of the nominal particle sizes for each powder is presented in Table 8. In addition, 1.5 wt% Licowax C was added to each mixture of the alloy to facilitate die compaction.

Table 8. Nominal particle sizes (microns) of the metallic powders utilized.

Powder	D_{90}	D_{50}	D_{10}
Aluminum	219	116	63
50:50 Al-Cu Master Alloy	76	36	13
Magnesium	48	32	14
Tin	36	16	6

3.3 Experimental Techniques

Blending of the metallic powders was done with a Turbula mixer in the following order: elemental aluminum was blended with the Al-Cu master alloy for 40 minutes, magnesium and tin were then added and blended for 45 minutes, and finally, Licowax C was added and blended for an additional 55 minutes. The powder blend was then die compacted in a floating die using an Instron 5594-200HVL load frame with a 1 MN load capacity. All samples were compacted at 200 MPa to form the required green part. Bars of two geometries were compacted in this fashion - transverse rupture strength (TRS) bars (31.7 x 12.7 x 10 mm) and charpy bars (75 x 12.7 x 12.7 mm). Green samples were then sintered in a three-zone tube furnace under a flowing nitrogen atmosphere (99.999%). The tube furnace was evacuated and back-filled with nitrogen twice before sintering to minimize the level of oxygen in the chamber. The thermal profile of the sintering process consisted of a 20-minute hold at 400°C for de-lubrication and a 20-minute hold at 630°C for sintering. Samples were then cooled to ambient within a water jacketed section of the furnace under flowing nitrogen. The temperature profile was recorded for each sinter by means of a type K thermocouple clamped on the sintering tray.

After sintering, samples were subjected to heat treatment and sizing. T1, T2, T3, T4, T6, and T8 treatments were all utilized. Table 9 describes the heat treatment and sizing processes applied in each instance.

Table 9. Descriptions of the tempers applied.

Temper	Description
T1	1. Naturally aged to stable condition at 21°C (minimum of 1 week)
T2	1. Sized at 200 or 450 MPa 1 hour* after sintering 2. Naturally aged to stable condition (minimum of 1 week)
T4	1. Solutionized @ 530°C for 2 hours 2. Water quench 3. Naturally aged to stable condition at 21°C (minimum of 1 week)
T3	1. Solutionized @ 530°C for 2 hours 2. Water quench 3. Sized at 450 MPa 1 hour after quenching 4. Naturally aged to stable condition at 21°C (minimum of 1 week)
T6	1. Solutionized @ 530°C for 2 hours 2. Water quench 3. Artificially aged @ 200°C for 10 hours
T8	1. Solutionized @ 530°C for 2 hours 2. Water quench 3. Sized at 450 MPa either 1 or 24 hours after quenching 4. Artificially aged @ 200°C for 10 hours

*The impact of various delay times was also investigated for the T2 condition.

Sizing of the sintered samples was completed using the Instron 5594-200HVL load frame at pressures ranging from 200 to 450 MPa. This targeted an OAL reduction of up to ~5.5% at 450 MPa. A closed die was used for sizing. To investigate the impact of delay time between sintering and sizing on the alloy, T2 samples were naturally aged for 1, 10, 100, and 1000 hours before sizing at 450 MPa. Densities were measured using an Archimedes approach based on oil infiltration as described in Metal Powder Industries Federation (MPIF) standard 42 [39].

Tensile data were obtained from machined threaded cylindrical tensile samples with a diameter of 5.00 mm (±0.05). The same Instron frame used for compaction and sizing was utilized for tensile testing, but when equipped with a 50 kN load cell rather than the 1 MN load cell. An Epsilon 3542 extensometer was used to measure engineering strain during testing. Samples were loaded at a rate of 2 MPa/s until fracture. Three samples were tested for each processing parameter and the average reported. A three-point bend fixture was used together with an Instron Model 1332 servo-hydraulic frame operated at 25Hz for fatigue testing. The fixture had a 24.7mm span between the lower pins that were made from hardened tool steel and had an outer diameter of 3.2 mm. TRS bars were tested in this fixture in accordance with the staircase method (runout of 1 million cycles; 5 MPa step size) to determine fatigue strength as described in MPIF Standard 56 [39]. TRS bars were pre-loaded to 0.1 kN and an R ratio of 0.1 was utilized. All TRS samples were de-burred prior to testing by light sanding on 600 grit SiC paper. No surface machining was carried out, to ensure that the sintered/sized surfaces were tested directly.

Optical micrographs of the unetched microstructures were obtained using a Zeiss Axio optical microscope. A scanning electron microscope (SEM) was also used to examine the microstructure. The SEM was a Hitachi S-4700 field emission instrument. Differential scanning calorimetry (DSC) was used to study heat treatment and precipitate development. A TA Instruments SDT Q600 V8.1 was used for these experiments. DSC samples were prepared by machining small cylindrical samples with a nominal diameter

and height of 4mm from TRS bars. Samples were heated in alumina crucibles from 50°C to 550°C at a rate of 10°C/min in air. A pure aluminum sample was initially tested and the resultant mass normalized heat flow was subtracted from the mass normalized trace acquired from each PM sample to isolate the thermal events related to precipitation-based reactions.

3.4 Results and Discussion

3.4.1 Naturally Aged Tempers (T1 and T2)

To test the impact that sizing had on the as-sintered alloy, mechanical testing was carried out on sintered (T1) and sintered + sized (T2) samples. Two process variables were explored: sizing pressure and the delay time between sintering and sizing. Two sizing pressures were tested that embody the range frequently encountered in commercial practice. Similarly, as sintered parts may sit for extended periods of time before they are sized, various delay times were tested. This would allow the sintered specimen to naturally harden to different extents prior to cold working (sizing), and therefore could change how sizing impacts the mechanical properties.

Figure 16-19 show the yield strength (YS) and ductility of the T1 and T2 samples. From these results, it was clear that increased sizing pressure led to higher YS, but lowered ductility at the highest sizing pressure considered. The impact of delay time between sintering and sizing was not as pronounced. Here, minimal changes in YS and ductility were observed even when delay time was increased to 1000 hours. With experimental

error taken into consideration, these transitions were viewed to be limited. Overall, sizing pressure was the more influential variable as it provided tangible gains in YS and modest reductions in ductility within T2 specimens.

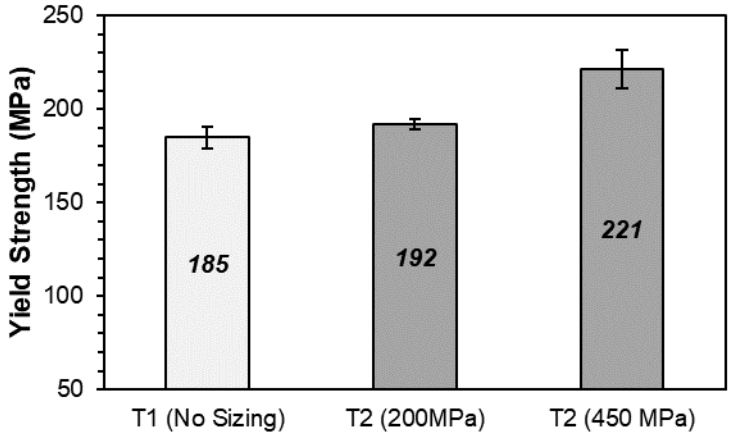

Figure 16. Impact of increasing sizing pressure on the yield strength of T1/T2 tempers. Average values indicated in bold italicized text. Sized samples have darker shading.

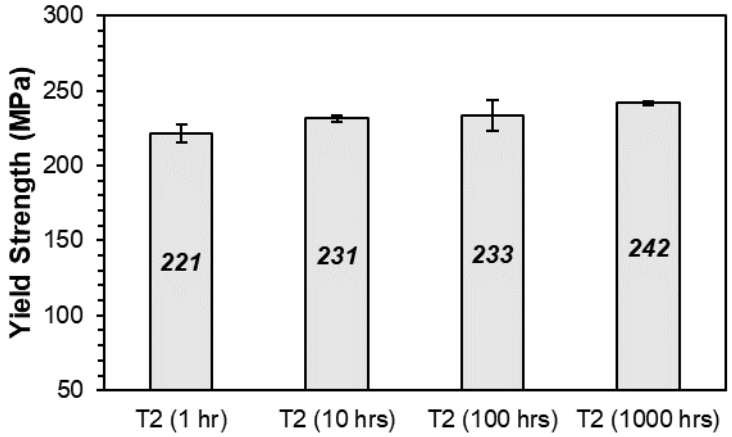

Figure 17. Impact of time delay between sintering and sizing on the yield strength of the T2 temper. Average values indicated in bold italicized text. All specimens sized at a pressure of 450 MPa.

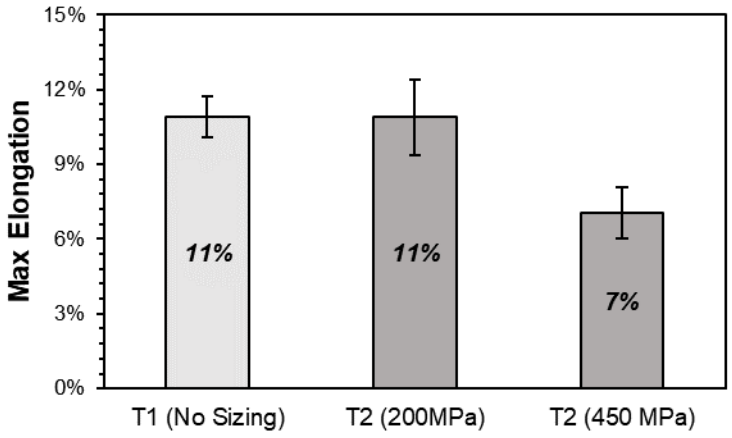

Figure 18. Impact of increasing sizing pressure on the ductility of T1 and T2 tempers. Average values indicated in bold italicized text. Sized samples have darker shading.

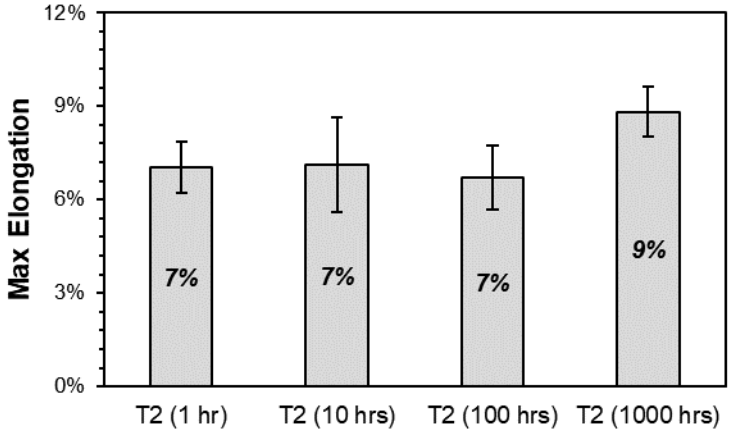

Figure 19. Impact of time delay between sintering and sizing on the ductility of T2 temper. Average values indicated in bold italicized text.

It was determined that sizing also had an impact on fatigue properties. As with the tensile tests, the impact of sizing pressure and delay time were again investigated. Figure 20 and 21 show the average fatigue strengths measured for the T1 and T2 samples. In all fatigue charts shown in this paper, the upper and lower ends of the error bars represent the $\sigma_{10\%}$ and $\sigma_{90\%}$ fatigue stress (stresses at which 10% and 90% of the samples will pass) respectively.

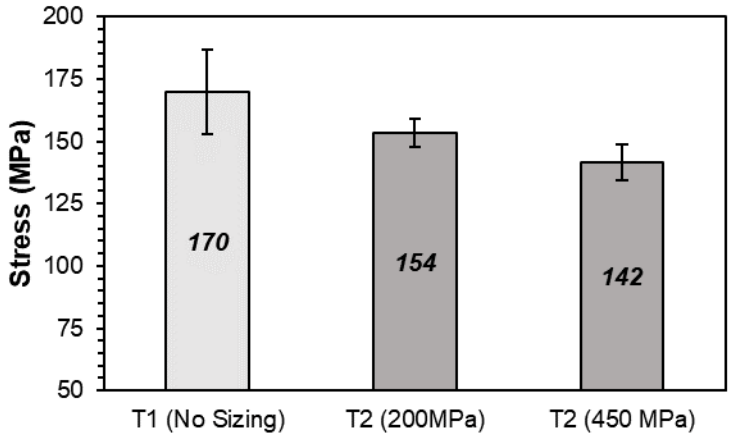

Figure 20. Impact of increased sizing pressure on the fatigue strength of T1 and T2 tempered specimens. Average values indicated in bold italicized text. Sized samples have darker shading.

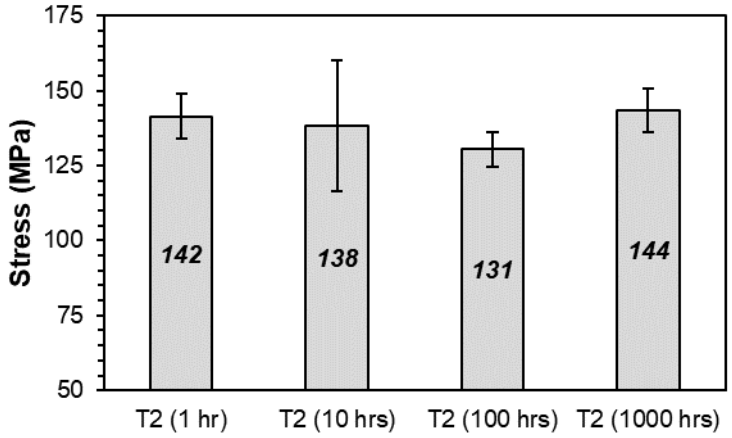

Figure 21. Impact of time delay between sintering and sizing on the fatigue strength of specimens in the T2 temper. Average values indicated in bold italicized text.

As sizing pressure increased, fatigue strength was negatively impacted. For example, when sized at 450 MPa, the fatigue strength of the alloy decreased by 16% when compared to the unsized (T1) processing route. This came as somewhat of a surprising result, considering the positive impact sizing had on yield strength. Figure 21 shows that increasing the delay time between sintering and sizing did not seem to have any significant impact on fatigue strength.

To determine why sizing negatively affected the fatigue properties of the alloy, microstructural analyses were completed. Optical micrographs of the unetched microstructures are shown in Figure 22 a-f. No significant differences in the microstructures were found that would signal why sizing had changed the mechanical properties. The images showed some residual porosity and the presence of secondary phases in all instances, but no cracks or other obvious abnormalities could be seen at any magnification. SEM analyses resulted in the same findings. Hence, it was hypothesized that the changes in mechanical properties arose due to variation(s) in precipitate development which could not be observed through either of the imaging techniques applied.

To gain insight into how precipitate development may have been affected by sizing, DSC trials were run on each of the T1 and T2 samples processed. Those pertaining to the effects of sizing pressure are shown in Figure 23. All traces contained peaks of an exothermic and endothermic nature that varied in position and magnitude as sizing was applied. As each peak corresponds to an event in the precipitation sequence of the S phase [27], it was concluded that sizing impacted precipitation hardening. The first endothermic effect occurred at ~230°C and was believed to be the dissolution Cu-Mg clusters and possibly S". This was followed by a relatively large exothermic peak ascribed to be the formation of the two variants of the S-phase precipitates; namely, S1 and/or S2. This peak occurred over a broad temperature range of 240°C to 410°C in the T1 sample. In sized specimens this peak shifted to lower temperatures, became narrower,

and more intense. It was also noted that these transitions became more acute as sizing pressure increased. These changes were believed to be due to the facts that S-type precipitates are known to preferentially nucleate on dislocations [37], and that the strain hardening instilled through sizing would introduce progressively higher concentrations of these defects as the applied pressure increased. This would have provided progressively higher concentrations of nucleation sites to facilitate precipitate formation, thereby shifting the peak to lower temperatures. It is also postulated that the width of the peak narrowed due to a preferential tendency to form S1 precipitates. This point is discussed in more detail at the end of the results section. Finally, there was a broad endothermic peak. Commonly denoted as a dissolution trough, this transition corresponded to the dissolution of S1 and/or S2 phases.

Additional DSC trials were then completed on T2 samples that were naturally aged for times of 1 hour and 1000 hours prior to sizing. The resultant heat flow data are shown in Figure 24. Both curves were in strong agreement, indicating that the S phase precipitate development was quite comparable in these specimens. This was consistent with the fact that the delay time between sintering and sizing did not impart any significant transitions in mechanical properties.

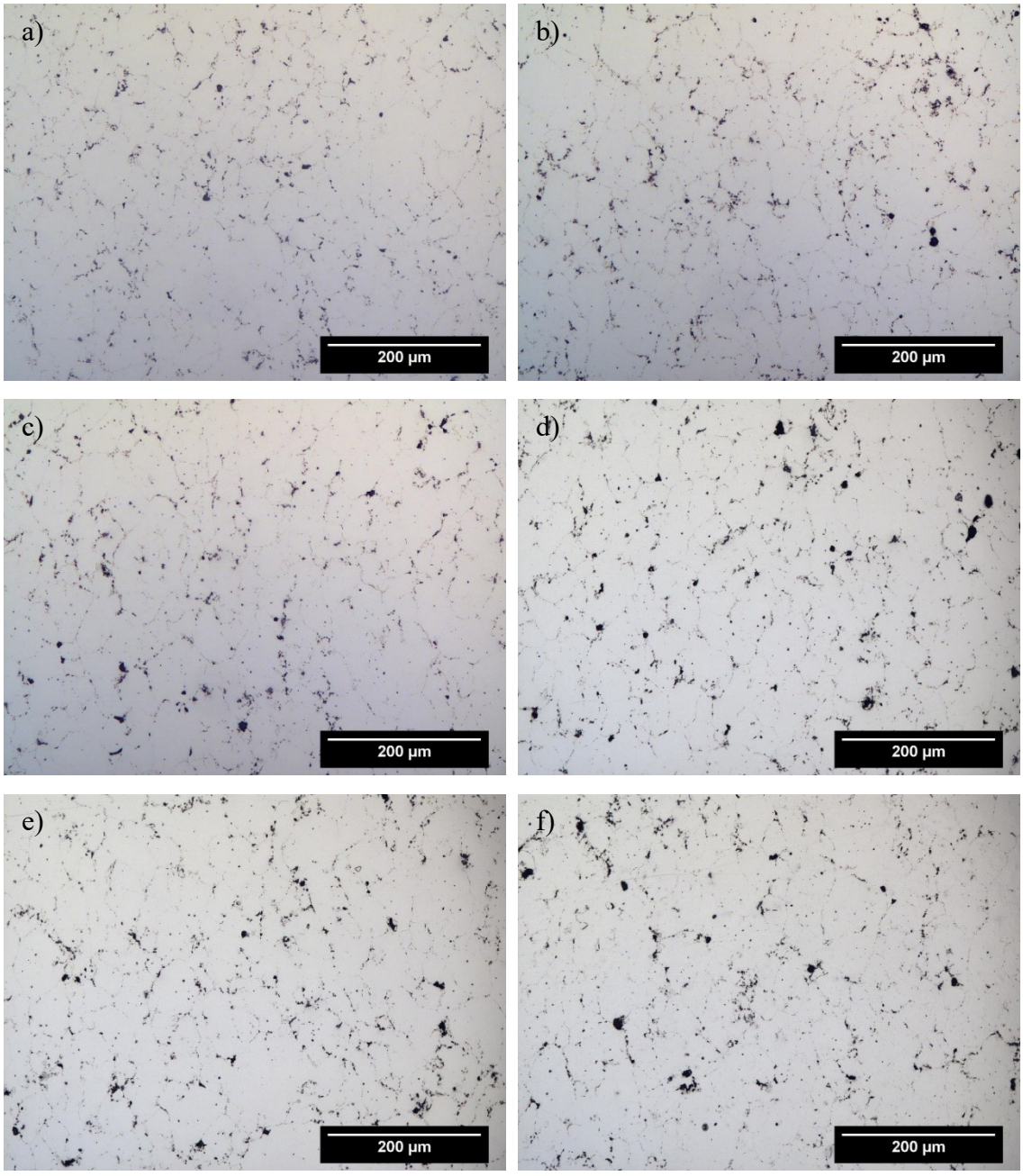

Figure 22. Optical images of the T1/T2 variants considered. a) No sizing, b) Sized at 200 MPa, c) Sized at 450 MPa, d) 10 hour delay time prior to sizing, e) 100 hour delay time prior to sizing, f) 1000 hour delay time prior to sizing.

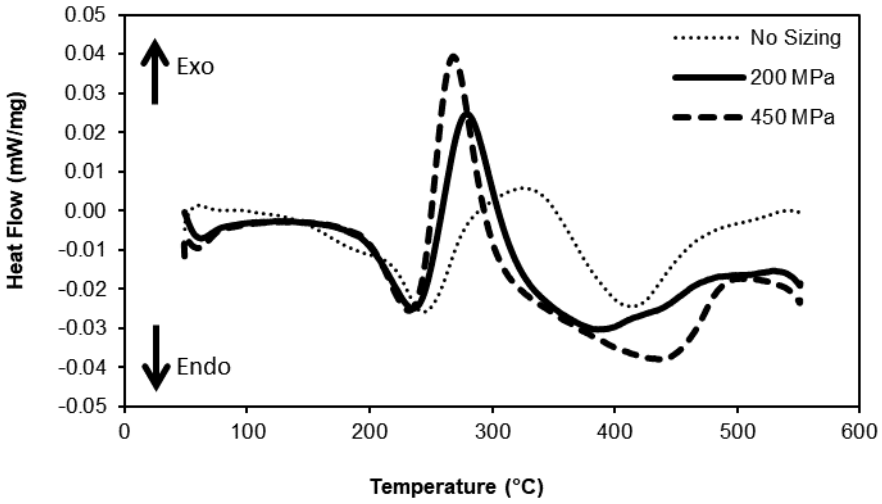

Figure 23. DSC traces acquired from specimens in the T1 and T2 tempers.

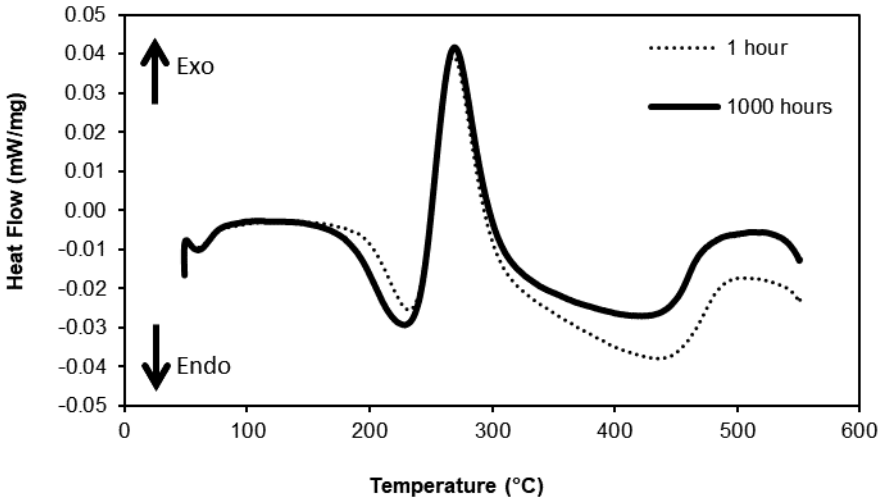

Figure 24. DSC traces acquired from samples in the T2 temper sized 1 hour and 1000 hours after sintering. Both specimens sized at 450MPa.

To gain an improved understanding of precipitate transitions during natural aging, a sintered specimen was solutionized at 530°C for 2 hours, water quenched, transferred directly to the DSC and heated. The resultant heat flow data are presented in **Figure** 25 along with the trace acquired from the T1 sample previously shown in Figure 23. A

notable distinction was that data from the quenched specimen exhibited an exothermic peak at ~110°C. This was believed to coincide with the first step in the S1/S2 reaction sequence – Cu-Mg cluster formation. This peak was not observed in any of the T1/T2 samples, indicating that the bulk of the precipitates in these specimens had already evolved to (or beyond) the cluster formation stage prior to heating in the DSC; in effect, during the natural age hardening period applied. Subsequent peaks coinciding with cluster dissolution, S1/S2 precipitation, and finally S1/S2 dissolution were remarkably like those generated from the T1 specimen in terms of their respective widths and temperatures of occurrence. As none of these peaks were shifted towards lower temperatures, this further substantiated the notion that sizing was in fact the driving force behind the transitions observed in Figure 23.

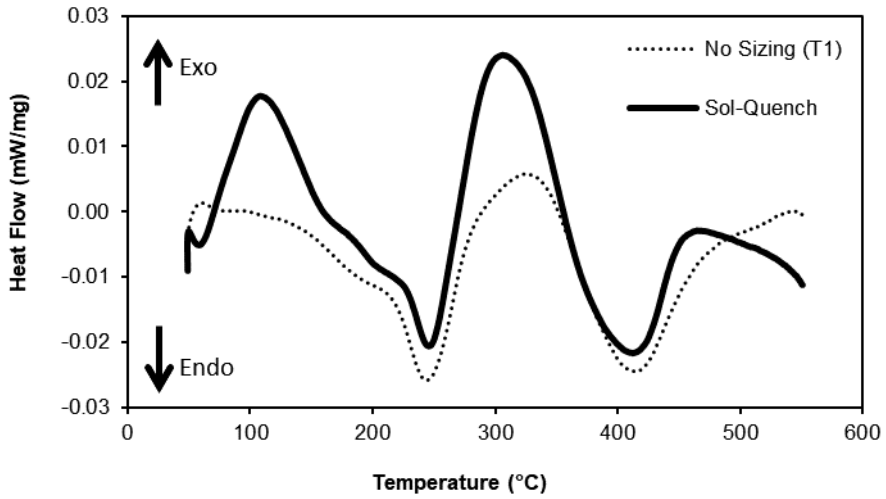

Figure 25. Comparison of the DSC traces acquired from a T1 sample and one that was heated immediately after being solutionized and water quenched.

3.4.2 Artificially aged Tempers (T6 and T8)

Solutionizing, quenching and artificially aging is commonly used in industry since it results in higher tensile strengths for 2xxx series aluminum PM alloys. For this reason, it was necessary to investigate if sizing had a comparable impact on T6/T8 tempered specimens of the alloy (i.e. positive on yield strength, yet negative on fatigue) relative to T1/T2 counterparts. Two variations on the T8 temper were investigated: one with a 1 hour delay between solutionizing and sizing, and another with a 24 hour delay between solutionizing and sizing. All T8 samples were sized at 450 MPa (~5.5% reduction) as this pressure was aligned with commercial practice and was found to have a prolific effect in accordance with T1/T2 data. Data on yield strength and ductility for the T6 and T8 samples are shown in Figure 26 and Figure 27 respectively.

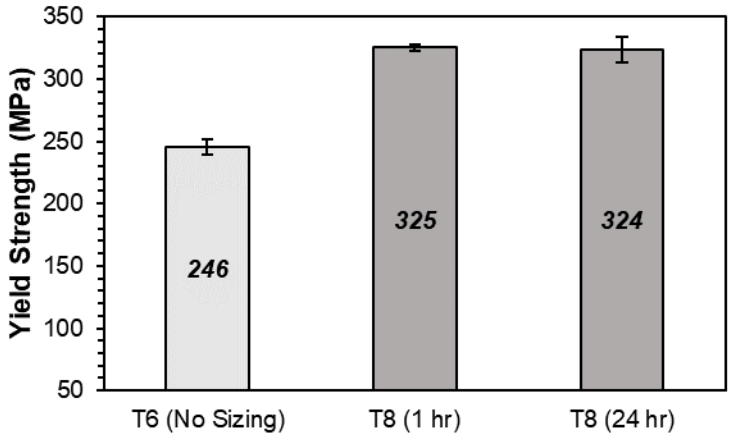

Figure 26. Comparison of the tensile yield strength measured for specimens in the T6 and T8(x) tempers. Average values indicated in bold italicized text. Sized samples have darker shading.

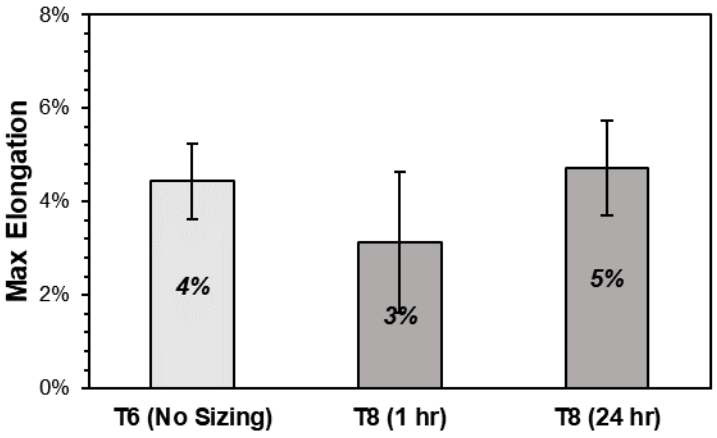

Figure 27. Comparison of the tensile ductility measured for specimens in the T6 and T8(x) tempers. Average values indicated in bold italicized text. Sized samples have darker shading.

Sizing increased the yield strength of the alloy by ~79MPa which equated to a net gain of 32% relative to the T6 counterpart. Conversely, a statistically relevant trend was not discernable when ductility data were assessed as all average values fell within a relatively narrow range of 3 to 5%. The delay time between sintering and sizing failed to bear an obvious impact on either property, suggesting that it was a factor of lesser influence. Relative to the T1/T2 specimens, those processed into the T6/T8 states offered enhanced yield strength at the expense of reduced tensile ductility.

Interestingly, sizing was again found to have a negative impact on the fatigue strength, as shown in Figure 28. Here, the T8 tempered products exhibited decreases in fatigue strength on the order of 25 to 30% when compared to those in the T6 temper. Although there may have been a slight increase in fatigue strength when the T8 samples were aged 24 hours before sizing, additional testing would be necessary to determine if this was a statistically meaningful change.

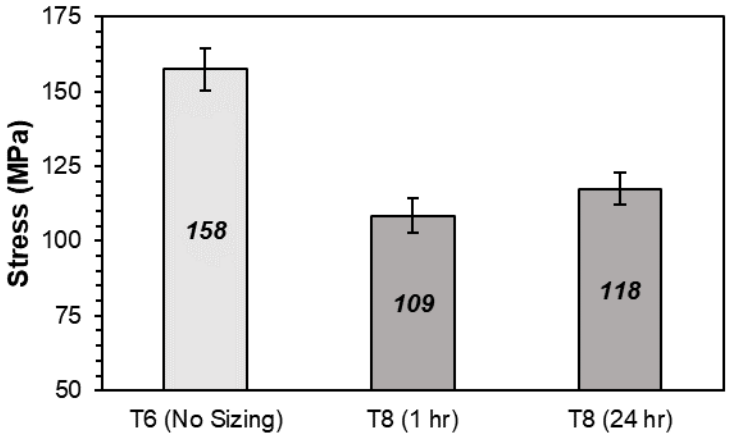

Figure 28. Comparison of the fatigue strength measured for specimens in the T6 and T8(x) tempers. Average values indicated in bold italicized text. Sized samples have darker shading.

As precipitate differences were found to underpin mechanical property differences in T1/T2 samples, DSC was again implemented to gain comparable insight on T6/T8 materials. Samples of T6, T8 (1 hour), and T8 (24 hours) were all run in the DSC, as shown in Figure 29.

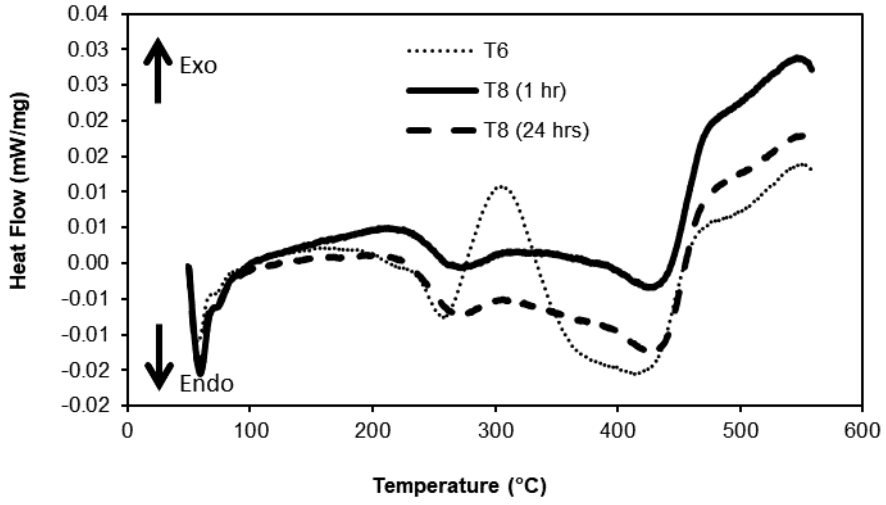

Figure 29. DSC heat flow traces acquired from T6 and T8(x) tempered specimens.

The T6 temper exhibited heat flow characteristics similar to those observed in the T1 temper in that peaks believed to coincide with cluster dissolution, S1/S2 precipitation, and S1/S2 dissolution were all observed. The largest peak was due to S1/S2 precipitation and occurred at 310°C. Interestingly, this peak was significantly diminished in both T8 samples, thereby indicating that most of the precipitates present in the T8 samples had already aged to the S1 or S2 state before heating in the DSC. This implied that precipitation reactions occurred more readily in the sized T8 samples. This was consistent with T1/T2 data in that sizing shifted the S1/S2 peak to significantly lower temperatures with sizing (Figure 23). Hence, it was evident that sizing had once again imparted a direct impact on precipitation and was therefore the underlying factor in the observed transitions in yield strength and fatigue resistance.

3.4.3 Solutionized, Quenched, and Naturally Aged Tempers (T3 and T4)

The final processing routes explored in this study were the T3 and T4 tempers. Here, select samples were solutionized at 530°C, quenched in room temperature water, and then naturally aged to a stable state to impart a T4 temper. The T3 temper was achieved by cold working (sizing) the samples immediately after quenching. Tensile data acquired from specimens in these tempers are shown in Figure 30 and 31.

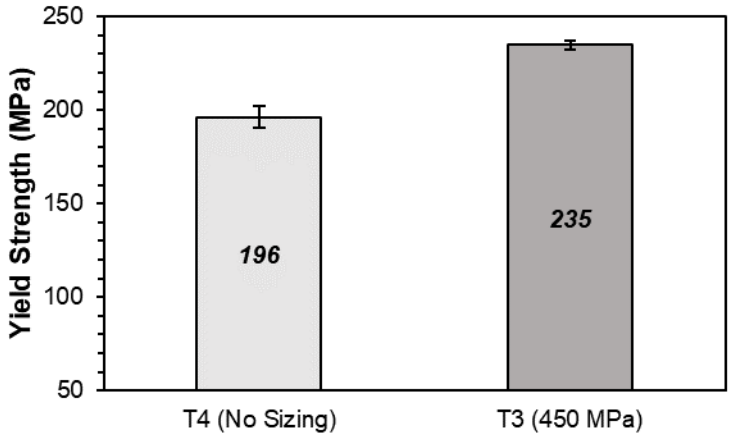

Figure 30. Comparison of the yield strength measured for specimens in the T4 and T3 tempers. Average values indicated in bold italicized text. Sized sample has darker shading.

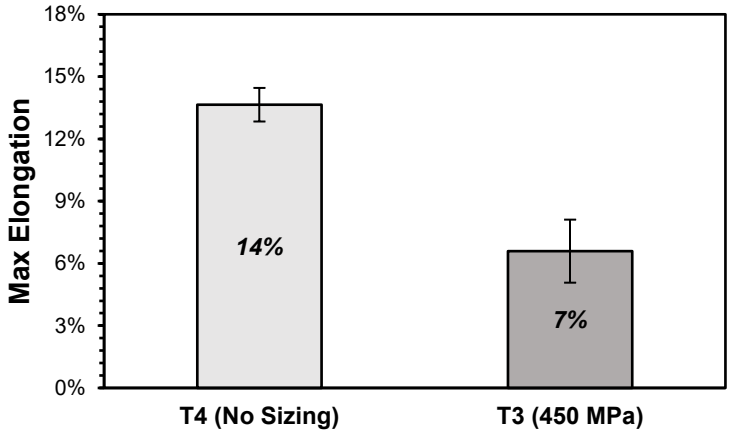

Figure 31. Comparison of the ductility measured for specimens in the T4 and T3 tempers. Average values indicated in bold italicized text. Sized sample has darker shading.

As expected, the sized (T3) samples exhibited a higher yield strength than those in the T4 state. This increase in yield strength came at the expense of ductility, which was halved in the sized temper. Overall, the T3/T4 samples displayed lower yield strengths, but higher ductilities than the T6/T8 samples. As with the other processing routes, fatigue strength was again negatively affected by sizing. Figure 32 shows that fatigue strength decreased

29% when the T3 temper was utilized. Interestingly, the T4 temper specimens displayed the highest fatigue strength of any processing route. These results align with what is commonly seen in wrought aluminum alloys in that T4 samples tend to have higher fatigue strengths and ductilities, whereas T6 samples tend to have higher yield and tensile strengths [32].

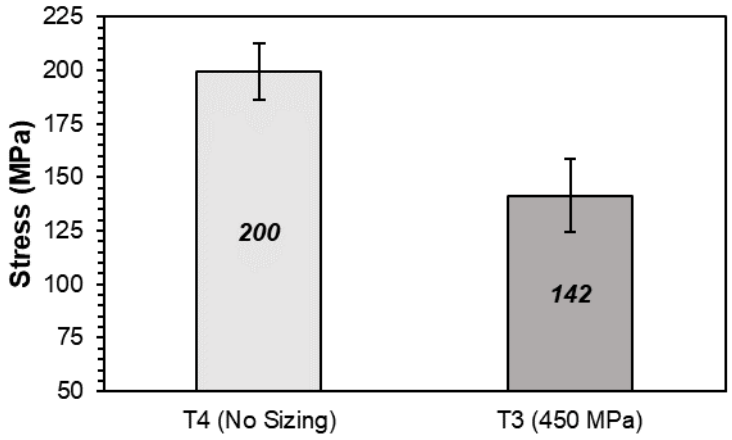

Figure 32. Comparison of the fatigue strength measured for specimens in the T4 and T3 tempers. Average values indicated in bold italicized text. Sized sample has darker shading.

Figure 33 shows the DSC results acquired from the T3 and T4 tempered materials. As with the other processing routes, the sized (T3) temper displayed a different heat flow trace than the non-sized counterpart. In particular, the principal exothermic peak of the trace was shifted to a lower temperature, was narrower, and more intense. As previously mentioned, all such transitions implied an intensified concentration of S1 precipitates nucleating on sizing-induced dislocations.

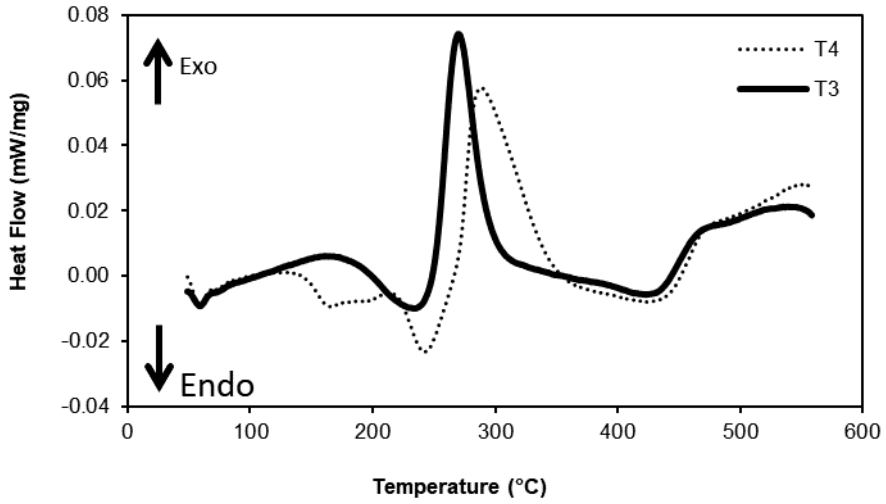

Figure 33. DSC heat flow traces acquired from T4 and T3 tempered specimens.

Table 10 shows an overall summary of averaged mechanical properties for all tempers explored in this study. In the case where multiple variations of the temper were assessed (T2 and T8), only the variation with the highest fatigue strength is shown. Considering all the different tempers, sizing consistently enhanced yield strength but negatively impacted fatigue response, and in general, tensile ductility.

Table 10. Summary of the average mechanical properties measured for the Al-2.3Cu-1.5Mg-0.5Sn PM alloy in the different tempers considered.

	Yield Strength (MPa)	Max Elongation (%)	Fatigue Strength $\sigma_{50\%}$ (MPa)
T1	185	10.9	170
T2	242	8.8	144
T4	196	13.6	200
T3	235	6.6	142
T6	246	4.4	158
T8	324	3.1	109

Based on the DSC results for all tempers, it was quite apparent that sizing had impacted precipitate development within the alloy. The DSC traces for all sized tempers (T2, T3,

and T8) were clearly distinguishable from the as-processed tempers (T1, T4, and T6). The principal difference in each case was related to the temperature at which the main exothermic peak (ascribed to S1/S2 formation) occurred and its width. Table 11 summarizes the transitions observed in this peak, as well as the peak width. For the T1/T2 and T3/T4 tempers (Figure 23 and Figure 33), DSC findings indicated that sizing consistently shifted this peak to a lower temperature, increased its magnitude, and decreased the peak width to a smaller temperature range. Similar peak shifts were seen by Wang and Starink [27] in AA2324 cold worked samples. Here it was concluded that in solution treated, quenched and subsequently cold worked samples, extensive formation of S1 occurs, whilst the formation of S2 was supressed. Other studies [28] also observed this peak shift under comparable circumstances. Interestingly, these researchers also observed a small exothermic effect on the shoulder of the S formation peak. They believed this to be associated with the formation of the S2 type precipitates. This shoulder effect was not observed in the T1/T2 and T3/T4 DSC results of this study because, according to Wang and Starink [27], only strain energy and interfacial energy are released during the transformation from S1 to S2, meaning that the expected heat effect associated with the transformation would be relatively small. This small heat effect from the transformation of S1 to S2 could be masked by the much larger heat effect of the S1 phase that forms at ~300°C in the samples that were not sized. Hence, although samples in the T1, T4, and T6 temper showed no signs of this shoulder effect, the S2 type precipitates were still believed to be present in these tempers. Conversely, it is proposed that the sized tempers likely have a higher concentration of the S1 precipitates which prompted a negative impact on fatigue resistance.

Table 11. Effect of sizing on the peak ascribed to S1/S2 precipitation.

	Peak Temperature		Peak Width	
Temper	No Sizing	Sized	No Sizing	Sized
T1/T2*	330°C	270°C	160°C	70°C
T6/T8**	310°C	240°C	100°C	80°C
T4/T3	300°C	270°C	120°C	70°C

* Value for sample sized at 450MPa
**Value for sample with 1 hour delay between solutionizing and sizing

Interestingly, the S1/S2 peak was effectively absent in DSC data from the T8 temper, which indicates that all the precipitates were already pre-aged to the S1/S2 state. This thereby implied that it was particularly easy to form S phase precipitates in this manner of heat treatment. The data given in Table 3 for the sized T8 sample is much more subjective than for the other tempers due to the nature of the S1/S2 peak in this case. Although not directly seen in the DSC trace, it is likely that the T8 temper, in much the same way as the T2 and T3 tempers, inhibits the formation of S2 precipitates and would therefore have a higher amount of the S1-type. Overall, the DSC traces for the T8 samples were significantly different from the T6 counterparts again indicating that sizing impacted the precipitate development.

3.5 Conclusions

In assessing the effects of sizing and heat treatment process on the PM alloy (Al-2.3Cu-1.5Mg-0.5Sn) of interest the following conclusions were reached:

1. Sizing led to meaningful increases in the tensile yield strength in all tempers, but this was accompanied by appreciable losses in fatigue resistance and tensile ductility.

2. The mechanical property transitions between unsized and sized specimens were found to scale with the applied sizing pressure.

3. The delay time between sintering and sizing did not impact mechanical properties significantly.

4. DSC assessments were consistently different for sized specimens (regardless of temper). In particular, the principal exothermic peak believed to be due to S1/S2 precipitation was shifted to lower temperatures, became narrower, and more intense. It was inferred that this signified a preferential tendency for the formation of S1-type precipitates in the sized specimens.

Chapter 4.0 Conclusions

This work attempted to determine how process variables (namely sizing and heat treatment) impacted the overall physical and mechanical properties of Al-2.3Cu-1.5Mg-0.5Sn. Of specific interest was the impact sizing had on fatigue properties and if the precipitates were influenced by the sizing process. The testing was carried out using various sizing pressures, heat treatment methods, and delay times between processing steps. The change in mechanical properties was quantified through uniaxial tensile testing and three-point fatigue testing. It was determined that sizing and heat treatment of Al-2.3Cu-1.5Mg-0.5Sn significantly influenced the mechanical properties. Sizing lead to similar changes in mechanical properties in samples that were both naturally and artificially aged.

Three different heat treatment methods were explored: naturally aged (T1 and T2), artificially aged (T6 and T8), and solutionized-naturally aged (T3 and T4). In all cases, sizing increased the tensile yield strength. The most significant increase was seen in the artificially aged tempers where the yield strength of the T8 (sized) samples was 32% higher than the T6 (not sized) samples. Conversely, sizing decreased the ductility in all cases. The largest decrease in ductility occurred in the solutionized-naturally aged tempers (T3/T4). In these samples, the maximum elongation was reduced from 13.6% in the not-sized temper (T4) to 6.6% in the sized temper (T3). This represents a 51% reduction in ductility. Delay time between sintering and sizing or solutionizing and sizing did not lead to a meaningful change in yield strength in any of the tempers studied.

The same three heat treatment methods were studied in the context of fatigue. In all cases, sizing led to a significant decrease in fatigue strength. The fatigue strength of the artificially aged samples was impacted the most. Here, sizing reduced the $\sigma_{50\%}$ fatigue strength by 31%. Delay time between sintering and sizing or solutionizing and sizing did not lead to a meaningful change in fatigue strength in any of the tempers studied.

Sizing of Al-2.3Cu-1.5Mg-0.5Sn affected the precipitation development of S-type precipitates. It was inferred through DSC assessments and literature review that sizing inhibited the transformation of S(type I) to S(type II). This would presumably lead to an increased amount of S1 precipitates in the sized samples and an increase in S2 precipitates in the not-sized samples. Because the influence of S1 versus S2 on the microstructure is different, it is proposed that this was a primary factor in the observed change in mechanical properties.

4.1 Future Work

Due to time and equipment constraints, there are numerous other studies that could be performed on this topic. Other research areas that could be explored include:

1. Using a TEM to observe the precipitates and see if there is in fact a higher concentration of S(type I) precipitates in the sized samples and a higher concentration of S(type II) in the non-sized samples.

2. Investigate the influence of solutionized-size-age versus size-solutionized-age. Determine if the timing of the sizing process has any influence in the properties of Al-2.3Cu-1.5Ng-0.5Sn.
3. Expand the scope of the study to other chemical compositions of Al-Cu-Mg-Sn and other 2xxx series aluminum PM alloys.
4. Investigate further into the impact of delay times between processing steps.

References

[1] German, R. M. (1984). *Powder metallurgy science*. Princeton, NJ: Metal Powder Industries Federation.

[2] Cooke, R. W., Hexemer, R. L., Donaldson, I. W., & Bishop, D. P. (2012). *Powder metallurgy processing of Al–Cu–Mg alloy with low Cu/Mg ratio*. Powder Metallurgy, 55(1), 29-35.

[3] Upadhyaya, G. S. (2002). *Powder metallurgy technology*. Cambridge: Cambridge International Science Pub.

[4] Neikov, O. D. (2009). *Handbook of non-ferrous metal powders: Technologies and applications*. Amsterdam: Elsevier.

[5] Material Technology Innovations Co., Ltd. (n.d.). Retrieved March 25, 2018, from http://www.mt-innov.com.

[6] Schaffer, G., Sercombe, T., & Lumley, R. (2001*). Liquid phase sintering of aluminium alloys*. Materials Chemistry and Physics*, 67*(1-3), 85-91.

[7] Kumar, V. (2011). *Simulations and modeling of unequal sized particles sintering* (Unpublished doctoral dissertation). University of Utah.

[8] Kubarsepp, J. (2016, January 15). *Technology of full density powder materials and products*. Lecture presented in Tallinn University of Technology.

[9] German, R. (1996). *Sintering theory and practice*. New York: Wiley.

[10] German, R. M. (1985). *Liquid phase sintering.* Springer US.

[11] Bishop, D., McNally Jr, R., & Geiman, T. (2000). *Metallurgical considerations in the manufacture and development of aluminum PM camshaft bearing caps*. Powder Metallurgy Aluminum & Light Alloys for Automotive Applications, compiled by W.F Jandeska and R.A. Chernenkoff, Metal Powder Industries Federation, Princeton, NJ, 2000, pp. 177-185.

[12] Zhou, J., Duszczyk, J. (1999). *Liquid phase sintering of an AA2014-based composite prepared from an elemental powder mixture*. Journal of Materials Science, 34(3), 545-550.

[13] Hasani, S., Panjepour, M., Shamanian, M. (2012) *The oxidation mechanism of pure aluminum powder particles*. Oxidation of Metals, 78 (3-4), 179-195.

[14] Yamasaki, M., & Kawamura, Y. (2006*). Changes in the surface characteristics of gas-atomized pure aluminum powder during vacuum degassing*. Materials Transactions, 47(8), 1902-1905.

[15] Kim Y. W., Froes, F.H. (1989). *Effect of surface oxides on processing and properties of high temperature aluminum powder alloys*. Advances in Powder Metallurgy, 3, 251-267.

[16] Lumley, R. N., Sercombe, T. B., & Schaffer, G. M. (1999). *Surface oxide and the role of magnesium during the sintering of aluminum*. Metallurgical and Materials Transactions A,30(2), 457-463.

[17] Schaffer, G., Hall, B., Bonner, S., Huo, S., & Sercombe, T. (2005). *The effect of the atmosphere and the role of pore filling on the sintering of aluminium.* Acta Materialia.

[18] Kaufman, J.G. (2000). *Introduction to aluminum alloys and tempers*. Materials Park, OH: ASM International.

[19] Judge W.D., Bishop, D.P, Kipouros G.J. (2017) *Effect of sizing on the corrosion behaviour of Alumix 123 P/M alloy in 3.5wt-% NACl solution*. Corrosion Engineering, Science and Technology, 52:1, 29-37.

[20] Boland, C., Bishop, D., Hexemer Jr, R., & Donaldson, I. (2010). *On the development of an aluminum PM alloy for "press-sinter-size" technology*. Conference paper, PowderMet2010.

[21] Bishop, D. P., Caley, W. F., Kipouros, G. J., Hexemer, R. L., & Donaldson, I. W. (2011*). Powder metallurgy processing of 2xxx and 7xxx series aluminium alloys*. Canadian Metallurgical Quarterly,50(3), 246-252.

[22] Perlitz, H., Westgren, A. (1943*). The crystal structure of Al_2CuMg*. Arkiv för kemi, mineralogi och geologi, 16.

[23] Grin, Y., Wagner, F., Armbruster, M., Kohout, M., Leither-Jasper, A., Schwarz, U., Wedig, U. Georg von Schnering, H. (2006). *CuAl2 revisited: Composition, crystal structure, chemical bonding, compressibility and Raman spectroscopy.* Journal of Solid State Chemistry, 179, 1709-1719.

[24] Kent, D., Schaffer, G. B., Drennan, J. (2005). *Age hardening of a sintered Al-Cu-Mg-Si-(Sn) alloy*. Materials Science and Engineering A 405, 65-73.

[25] Bagaryatsky, Y.A., 1952. *Structural changes on ageing Al-Cu-Mg alloys*. Doklady Akademii Nauk SSSR. 87, 397-401.

[26] Kovarik, L., Court, S., Fraser, H., Mills, M. (2008). *GPB zones and composite GPB/GPBII zones in Al–Cu–Mg alloys*. Acta Materialia*, 56*(17), 4804-4815.

[27] Wang, & Starink. (2007). *Two types of S phase precipitates in Al–Cu–Mg alloys*. Acta Materialia, *55*(3), 933-941.

[28] Parel, T.S., Wang, S.C., Starink, M.J. (2010), *Hardening of an Al-Cu-Mg alloy containing Types I and II S phase precipitates*. Materials and Design, 31, S2-S5.

[29] Schaffer, G., Yao, J., Bonner, S., Crossin, E., Pas, S., & Hill, A. (2008). *The effect of tin and nitrogen on liquid phase sintering of Al–Cu–Mg–Si alloys*. Acta Materialia, 56(11), 2615-2624.

[30] Cooke, R., Hexemer, R., Donaldson, I., & Bishop, D. (2015). *Press-and-sinter processing of a PM counterpart to wrought aluminum 2618*. Journal of Materials Processing Technology, 230, 72-79.

[31] Boland, C., Hexemer, R., Donaldson, I., & Bishop, D. (2013). *Industrial processing of a novel Al–Cu–Mg powder metallurgy alloy.* Materials Science and Engineering: A, 559, 902-908.

[32] Smithells, C., Brandes, Eric A., & Brook, G. B. (1998). *Smithells light metals handbook*. Oxford (England) ; Boston: Butterworth-Heinemann.

[33] Harding, M., Donaldson, I., Hexemer Jr, R., Bishop, D.P. (2017). *Effects of post-sinter processing on an Al–Zn–Mg–Cu powder metallurgy alloy*. Metals, 7(9), 370.

[34] Cooke, R.W., Steedman, G., Bishop, D.P., Hexemer Jr, R.L., Donaldson, I.W. (2013*). Preliminary studies on the development of hot-forged aluminum PM technology*. Conference paper, PowderMet 2013.

[35] Grayson, G.N., Schaffer, G.B., Griffiths, J.R. (2004). *On the fatigue on sintered aluminum alloys*. Materials Forum. 28, 981-985.

[36] Jena, A.K., Gupta, A.K., Chaturvedi, M.C. (1989). *A differential scanning calorimetric investigation of precipitation kinetics in the Al-1.53 wt% Cu-0.79 wt% Mg alloy*. Acta Metallurgica. 37, 885-895.

[37] Wilson, R.N., Partridge, P.G. (1965*). The nucleation and growth of S' precipitates in an aluimum-2.5% copper-1.2% magnesium alloy*. Acta Metallurgica. 13, 1321-1327.

[38] Styles, M.J., Marceau, R.K.W., Bastow, T.J., Brand, H.E.A., Gibson, M.A., Hutchinson, C.R. (2015). *The competition between metastable and equilibrium S*

(Al2CuMg) phase during the decomposition of Al-Cu-Mg alloys. Acta Materialia. 98, 64-80.

[39] Metal Powder Industries Foundation (2012). *Standard test methods for metal powders and powder metallurgy products, standard 42*. MPIF, Princeton, NJ.